Improving wind tunnel '1-cos' gust profiles

Davide Balatti*, Hamed Haddad Khodaparast†, Michael I. Friswell, ‡
Swansea University, Faculty of Science & Engineering, Bay Campus, Swansea, SA1 8EN, United Kingdom

Marinos Manolesos§
City, University of London, Northampton Square, London EC1V 0HB, United Kingdom

A vane type gust generator has been designed and characterized in the Swansea University wind tunnel to enable the validation of the response of aircraft models to gust loads. The experimental results reveal the complexity of the flow between the gust vanes and the aircraft model location. Previous studies have shown that generating a predetermined gust profile at the desired location in the wind tunnel is a challenging problem. In this work, two techniques to improve the '1-cos' gust have been considered. In the first case, the transfer functions between the vane rotation and the gust produced at the aircraft model location have been identified, and its inverse has been used to calculate the vane rotation. The strong aerodynamics nonlinearity limits the improvements of this method. A parametric study on vane rotation has shown that a more complicated vane rotation function made it possible to obtain '1-cos' gusts at the aircraft model location with a mean square error two orders of magnitude smaller than the initial case. Creating '1-cos' gusts with similar frequency content as the regulations require will help design more efficient gust load alleviation systems.

Nomenclature

A	=	maximum vane deflection
B	=	coefficient of the growing exponential curve
c	=	vane chord
C	=	coefficient of the decaying exponential curve
f	=	vane frequency rotation
F_g	=	flight profile alleviation factor
H	=	gust gradient
$H(s)$	=	transfer function

*PhD student in the Department of Aerospace Engineering
†Professor in Aerospace Engineering
‡Professor Emeritus in Aerospace Engineering
§Reader in Aerospace Engineering

k = reduced frequency

K = gain factor of the transfer function

l_g = gust wavelength

n = negative peak factor

p = pole of the transfer function

s = Laplace variable

t = time

t_{conv} = convection time

t_{s} = shedding time

t_{ss} = sinusoidal excitation shedding time

t_{ss}^{i} = identified sinusoidal excitation shedding time

t_{01} = delay of the '1-cos' vane rotation

t_{02} = time for the unit value of the decaying exponential curve

t_1 = time at Point 1

t_2 = time at Point 2

t_3 = time at Point 3

U = horizontal airspeed

V = vertical airspeed

V_∞ = free stream velocity

w_g = gust

w_{g_0} = maximum gust velocity

w_{ref} = reference gust velocity

z = zero of the transfer function

α = angle of attack

α_{min} = minimum angle of attack

α_{max} = maximum angle of attack

θ = vane rotation profile

τ = delay of the transfer function

τ_f = time delay between sinusoidal rotation

ω = angular frequency

I. Introduction

The need for more efficient aircraft has forced researchers to look for more advanced aircraft configurations in recent decades. The use of more advanced structural materials, such as composite materials, and the aerodynamic design based on a higher aspect ratio wings improve both weight and aerodynamic terms in the classical Breguet equation [1]. The increase in aerodynamic and structural performance has grown together with more sophisticated flight control systems. Designers have implemented maneuver and Gust Load Alleviation (GLA) technologies to reshape the wing load distribution [2]. Gust loads are among the most critical cases an aircraft can encounter. Researchers have been looking for strategies to reduce structural stresses at the wing root caused by gust encounters, either by using active methods (e.g. active control surfaces) [3] or passive (e.g. aeroelastic fiber and thickness tailoring) [4].

Active GLA is not a new topic; for example, in 1974 investigations were performed on the Lockheed C-5A fatigue issues leading to the development of the "Active Lift Distribution Control System" [5]. Initially, GLA was implemented either to fix a developing problem or to provide enhancements to existing aircraft. Aeroelastic modeling for gust response is a relatively mature technology and is a crucial element during the design of new aircraft. The structure of recent flexible and lighter-weight aircraft has become more elastic, and the separation between flexible and rigid body modes has been reduced. Therefore flutter suppression, gust load alleviation, and flying qualities need to be treated simultaneously [6]. For a more accurate GLA system in future aircraft, techniques for turbulence and gust identification using simulated in-flight data have been proposed [7].

While GLA plays a crucial role, huge efforts have been made to find techniques that reduce aerodynamic drag. A considerable contribution, usually 30%-40% of the overall drag, is a lift-induced drag, which could be reduced by increasing the wingspan. However, such a design solution has some limitations related to the maximum aircraft dimensions allowed at airports and also to the increase in bending moments along the wing. A possible solution to the first problem is to use a folding wing that can be employed on the ground. An example of this technique is the latest version of the Boeing B777X, which, through the use of wingtips the wingspan will be 7 meters longer than that of the original B777. The folding wingtip capability will be used only on the ground during taxi to and from the gates allowing the aircraft to fit within the airport gate. The concept of folding wingtips has been used on a number of aircraft [8]. Recently numerical models [9, 10] and experimental works [11, 12] have proven the capability of a zero stiffness flared hinge to alleviate the gust loads.

The unsteady nature of a gust and strong coupling between the resulting aerodynamic loads and structural deformations make the modelling process quite complex. Analysing the performance of a GLA system through flight tests has some drawbacks. Indeed, to evaluate the system performance, it is difficult to find the proper turbulence

Presented as Paper with the title "Improving wind tunnel '1-cos' gust profiles" at the 2022 AIAA SciTech Forum, San Diego, CA, 3-7 January 2022

conditions or extreme gusts because, by definition, extreme gusts are sporadic. The artificial generation of atmospheric turbulence and gusts is a complex task, and a possible approach could be flying in the wake of an aircraft. The phenomenon of encountering wakes has some peculiarities to the gust and turbulence encountered and can be considered a problem on its own [13, 14]. The measurement of gust disturbance acting during flight tests is a challenging task. Due to the impossibility of controlling the variables of interest, it is difficult to replicate the same test without the GLA system and with different control strategies. Experiments are possible with full-scale aircraft and models.

The experimental validation of active or passive control technologies on scaled aeroelastic models is a challenging task [3, 15] and requires specific equipment in the wind tunnel. Active grids are commonly used in wind tunnels to generate turbulence but cannot generate discrete large amplitude gusts. The construction of a gust generator is required for gust loads experiments in a wind tunnel. The first documented attempt to produce gusts in the wind tunnel was in 1966 at the National Aeronautics and Space Administration's (NASA) Langley Research Center by Richard et al. [16]. Due to limitations in the vane amplitude or frequency to create discrete gusts and the inability to separate transverse and longitudinal gust components, they decided to inject air to induce pure longitudinal oscillations in a wind tunnel stream. The air was stored in a 56.6 m^3 tank and electrovalves were used to modulate the air supplied to the four injectors. They showed the ability of the air injection technique to generate longitudinal gusts in the wind tunnel. In 1969 Buell et al. [17] proposed cascade oscillation vanes to produce longitudinal gusts. In contrast with the previous designs, this concept allows large Reynolds numbers and turbulence scales appropriate for large structures. Velocity measurements downstream from the vanes demonstrated that gusts in either the longitudinal or the lateral directions can be generated. Different configurations have been considered in the past 50 years, driven by experimental requirements and the available wind tunnel facilities [18, 19]. A review of existing gust generators installed around the world is given in [18]. Most gust generators are based on one or multiple pitching airfoils [17–29]; however, alternative solutions exist. In 1981 Reed et al. [30] built a gust generator for the Transonic Dynamic Tunnel using small pitching surfaces mounted on the sidewall of the tunnel. The vanes did not span the entire test section width. The vane trailing vortices induce a vertical velocity component across the model suspended in the center by cables. Tang et al. [31] used four vanes with a rotating slotted cylinder at the trailing edge to reduce the mechanical complexity and increase the controllability and reliability of a gust generator. Results showed the ability of this technique to produce controllable harmonic gusts requiring very low torque. However, this technique's maximum gust angle is lower than that obtained by pitching vanes. To study the behavior of small-scale micro aerial vehicles and small birds Roadman et al. [32] used an active grid to generate continuous turbulence following the Makita style [33]. This design cannot produce '1-cos' gusts as prescribed by the certification authorities [34]. Allen et al. [26] built a gust generator at the Aircraft Research Association (ARA) to operate under transonic flow conditions, within a large wind tunnel section, by blowing air jets mounted on two fixed profiles. Experimental works have shown the ability of multiple oscillating aerofoils to produce continuous sinusoidal gusts [18–20, 22, 25]. The creation of single '1-cos' gusts has been shown to be a challenging

problem. Indeed, experimental single '1-cos' gusts are characterized by undesired negative peaks before and after the main positive peak [19, 20, 27].

This work had two objectives: first, the design, installation, and commissioning of a gust generator in the Swansea University wind tunnel and, consequently, finding techniques to improve the creation of '1-cos' gusts. When a 'perfect' '1-cos' gust profile is produced in the wind tunnel, the comparability between data from different facilities and experiments and simulations is significantly improved. In addition, standardization, benchmarking, simulation validation, and reproducibility are improved when a 'book' case is correctly reproduced experimentally. First of all, in Section II desired gusts, as well as the gust generator design with the component selected, are introduced. Section III discusses hot-wire anemometer, vane rotation profile, and post-processing technique. In Section IV, discrete and continuous sinusoidal gusts and flow uniformity measurements are presented along with the main reason behind the discrepancy between the desired and the measured '1-cos' gusts. Two innovative techniques to improve the discrete gusts are discussed, and the results are shown in Section V, before the conclusions are given.

II. Gust generator design

The aim of the gust generator is to create gusts according to the CS25 certification from the European Aviation Safety Agency [34]. Atmospheric disturbance models are categorized into two idealized categories: discrete gust and continuous turbulence. In this work, single ('1-cos') gusts and continuous sinusoidal (harmonic) gusts are considered. '1-cos' gusts are defined as

$$w_g(t) = \begin{cases} \frac{w_{g_0}}{2}\left[1 - \cos\left(\frac{2\pi V_\infty}{l_g} t\right)\right] & \text{for} \quad 0 \le t \le \frac{l_g}{V_\infty} \\ 0 & \text{for} \quad t > \frac{l_g}{V_\infty} \end{cases} \tag{1}$$

where w_{g_0} is the maximum gust velocity of a gust with wavelength l_g and airspeed V_∞. For the case of civil commercial aircraft, gusts wavelengths are varied between 18 m to 214 m (according to [34]) and the gust velocity is calculated as

$$w_{g0} = w_{\text{ref}} F_g \left(\frac{H}{107}\right)^{1/6} \tag{2}$$

where the gust gradient H is half the gust wavelength l_g and F_g is the flight profile alleviation factor, which increases linearly from sea level to 1.0 at the maximum operating altitude. w_{ref} is the reference gust velocity, which reduces linearly from 17.07 m/s Equivalent Air Speed (EAS) at sea level to 13.41 m/s EAS at 4572 m, and then again to 6.36 m/s EAS at 18288 m. Figure 1 shows gusts at different wavelengths at 200 m/s and sea level.

Discrete gusts can be seen as a realistic impulse excitation for an aircraft. The duration of the impulse influences the frequency content of the impulse response. Figure 2 shows the Fourier transform of the discrete gusts with a maximum

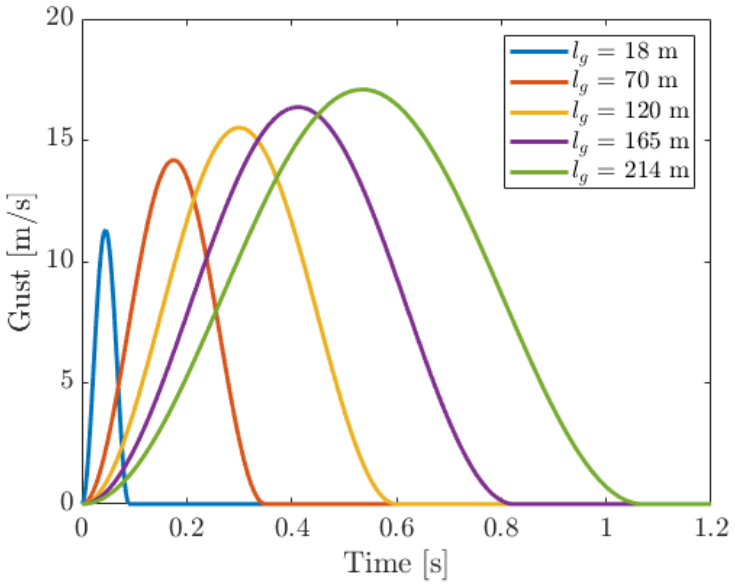

Fig. 1 *Discrete gust with different gust wavelengths at* 200 *m/s airspeed*

amplitude of 20 m/s and gust wavelengths of 40 m and 20 m at an airspeed of 200 m/s, which corresponds to 5 Hz and 10 Hz for 40 and 20 m, respectively. The range of frequency with a flat frequency content is inversely proportional to the duration of the impulse, which in this case, is the gust length. Indeed, a discrete gust with a high gust length mainly excites aircraft's rigid body modes, while a discrete gust with a small gust length excites aircraft's rigid body modes and elastic modes. In the rest of this work, discrete gusts are described in terms of maximum amplitude and frequency, where the frequency is defined as the inverse of the impulse duration.

Figure 3 shows the Swansea University wind tunnel, which is a closed section, a closed-circuit system with a test section of 1.5 m by 1 m and a length of 2.36 m. It has temperature control and an airspeed control system that allows working velocities between 10 m/s to 50 m/s.

The GG should be able to produce continuous and discrete gusts with a maximum frequency of 14 Hz and amplitude range from 5° to 20°. The design of the gust generator, e.g., number of vanes, vane profile, chord and span dimensions, the separation between vanes, and actuation type, have been selected based on suggestions given in [19, 27] and engineering judgment. As discussed in [27], increasing the number of vanes could increase the maximum gust angle and lead to a more uniform gust field in the wind tunnel, but it would increase the blockage in the test section. Moreover, the flow in the test section would be affected by the wakes of the vanes [27]. Vanes with a higher chord dimension could produce gusts with higher intensity, but increasing the chord dimension will increase the inertia and the torque required to rotate the vanes. Reducing the vertical separation between the vanes could produce more significant gusts. However, for future aeroelastic testing of wings subjected to gusts, a small vertical separation would reduce the working height [19]. Considering the Swansea University wind tunnel size, two horizontal vanes were used to cover the entire

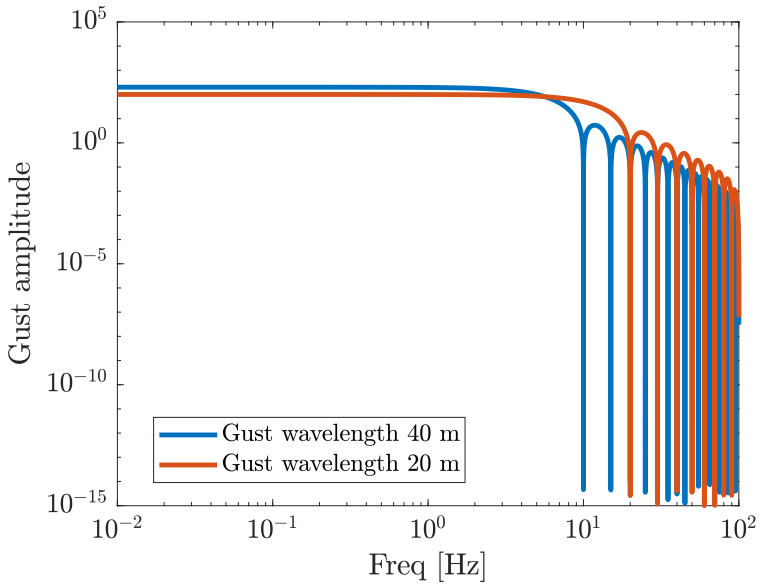

Fig. 2 *Frequency content of discrete gust with different gust wavelengths at* 200 *m/s airspeed*

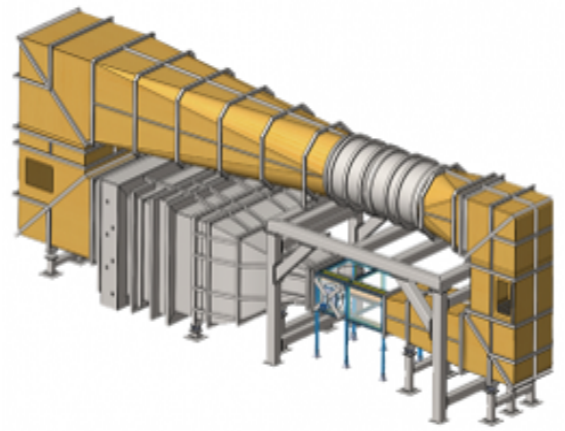

Fig. 3 *Swansea University wind tunnel*

width of the chamber. A NACA0015 profile with a 200 mm chord was chosen to have a symmetric airfoil, limiting the thickness but allowing a spar to fit inside. For manufacturing simplicity, 3D printed vanes were used. The rigidity of each vane was ensured by a hardened steel shaft to which the 3D printed vanes were bonded at the quarter chord to limit the aerodynamic and structural coupling. Each vane consists of eight sections due to the 3D printer size limitations. Each vane is controlled with a separate servomotor to rotate each vane with any prescribed motion. A low backlash gearbox was introduced between the vane and the motor to reduce the required motor torque and increase the motor rotation. The motion requirements in terms of frequency range and maximum amplitude have been decided based on a similar design [19, 34].

The gust generator has been designed to create single and continuous sinusoidal gusts. Table 1 reports the main vane proprieties. Figure 4a shows the two vanes used. Figure 4b shows the vanes connected to the respective servomotor

Vane material	ABS
Chord	200 mm
Span	1500 mm
Airfoil profile	NACA0015
Spar material	16 mm diameter hardened steel shaft
	Young's modulus 210 GPa
	Density 7850 kg/m^3

Table 1 *Vane design and dimensions*

through a gearbox. Figure 4c shows the vanes installed in the wind tunnel. The gust generator has been located at the start of the wind tunnel test section to have enough space to fit future models for wing gust experiments. Table 2 shows the components selected for the drives, motors and gearboxes.

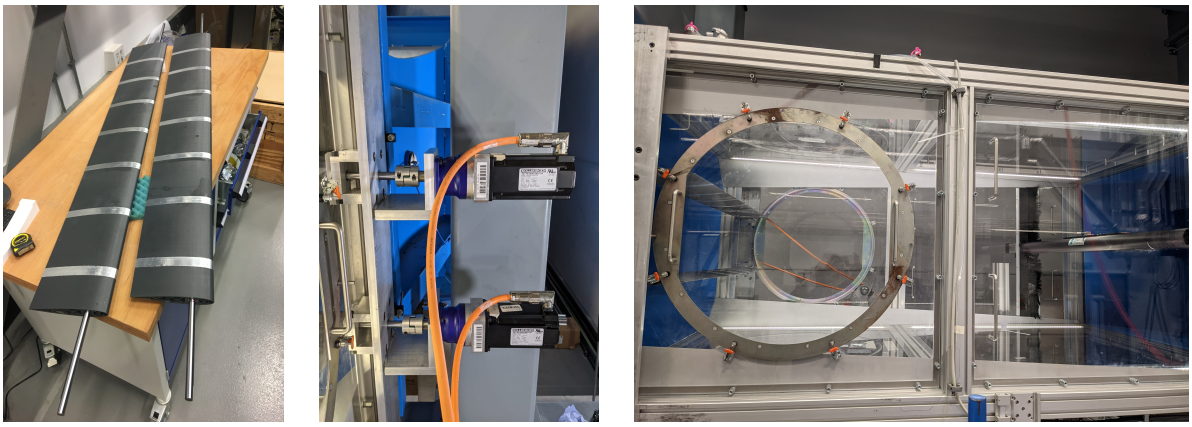

(a) **(b)** **(c)**

Fig. 4 *Vanes* (a)*, motors and gearboxes* (b) *and vanes in the wind tunnel* (c)

Drive	Kollmorgen AKD-P00306
Motor	Kollmorgen AKM43E
	Maximum torque 40 Nm
Gearbox	Wittenstein SP+075-MF1-10-1XX
	10:1 ratio, backlash 2 arcminutes

Table 2 *Gust generator components*

A. Vane structural characterisation

Structural dynamic characterisation has been performed to assess the first natural frequency of the vane installed in the wind tunnel. Knowing the first vane natural frequency allows the identification of oscillations in the gust profile due to the vane vibration. The first natural frequency has been identified by hammer test at 19.7 Hz.

III. Experimental setup

A cross hot-wire sensor has been used to measure the horizontal (parallel to the free stream) and vertical components of the flow field for all the measurements. In all the tests, the sampling frequency has been kept at 1 kHz. The hot-wire anemometer has been placed in the center of the cross-section, at the longitudinal distance of 1.234 m from the vane trailing edge (corresponding to 6.2 chords), where future wings will be set to measure the wing gust response. A 0.3 m stainless steel tube was used as a probe extension to prevent the interference of the probe support on the measurements.

A. Test cases

A series of wind tunnel tests have been performed to assess the ability of the gust generator to produce single and continuous sinusoidal gusts. In the case of discrete gusts, the shape of the desired gusts is described by Eq. (1), so the vane rotation profile $\theta(t)$ was set to follow a similar movement according to

$$\theta(t) = \begin{cases} \frac{A}{2}\left[1 - \cos(2\pi f t)\right] & \text{for} \quad 0 \leq t \leq \frac{1}{f} \\ 0 & \text{for} \quad t > \frac{1}{f} \end{cases} \tag{3}$$

where A is the maximum deflection of the vanes in degrees and f is the frequency in Hertz. The free stream velocity ranged from 10 m/s to 26 m/s. This corresponds to Reynolds numbers in the range of $2.45 \cdot 10^5$ to $6.4 \cdot 10^5$ considering the vane chord as characteristic length. In the tests, the vane maximum pitch amplitude ranged from 5° to 20° in 5° increments, while the vane rotation frequency ranged from 1 Hz to 14 Hz. Higher pitching frequencies were avoided to avoid excessive vane vibrations. The maximum reduced frequency is $k = 0.88$, where k is defined as

$$k = \frac{\omega c}{2V_\infty} \tag{4}$$

where $\omega = 2\pi f$, c is the vane chord and V_∞ is the free stream velocity.

In the case of continuous sinusoidal gusts, the vane rotation profile was set to follow a sinusoidal trajectory, defined as

$$\theta(t) = A\sin(2\pi f t) \tag{5}$$

In this case, the free stream velocity ranged from 10 m/s to 18 m/s, the maximum vane amplitudes are 5° and 12.5°, and the vane rotation frequency varied from 1 Hz to 10 Hz. At the highest rotational speed, the reduced frequency is $k = 0.63$. The main objective of this work was to improve the creation of discrete gusts, and so continuous sinusoidal gusts have been considered for only a limited set of airspeed and frequency.

B. Post-processing

The effect of the gust has been considered as a temporary change of the angle of attack, calculated as

$$\alpha = \text{atan}\left(\frac{V}{U}\right) \tag{6}$$

where V and U are the vertical and horizontal airspeeds measured by the cross hot-wire sensor. The measured data have been filtered using a low-pass filter and a notch filter. The measurement from the hot-wire sensor introduces noise at all frequencies. Therefore, the low-pass filter is required to attenuate the high-frequency noise. As the gust generator will be used to measure the gust response of wings characterized by low aeroelastic frequencies, which would act as a low pass filter, it is expected that higher frequencies will have a negligible impact. The cut-off frequency was set to 20 Hz. The natural frequency of the probe joined to the probe extension was experimentally identified at 25 Hz. A notch filter with a central rejected frequency of 25 Hz has been used to reduce the noise due to the probe extension vibrations.

IV. Initial results

This section presents the results for the discrete gusts and continuous sinusoidal gusts. Figure 5 shows the measured gust and the filtered gust. The oscillations at 25 Hz before and after the main peaks and the high-frequency oscillations have been filtered out. Figure 6 shows the measured angle of attack repeated three times, measured when the vane rotation amplitude is 10°, the frequency is 8 Hz, and the airspeed is 14 m/s. The maximum standard deviation of the measurements is 0.14°, and it is at the maximum peak.

A. Discrete gust

Figures 7 and 8 show the measured flow angles at different airspeeds and pitching amplitude. The results show that increasing airspeed reduces the maximum peak while increasing the pitching frequency or increasing the pitch amplitude causes the peak to increase. Figure 8 shows that varying the airspeed or maximum vane rotation amplitude,

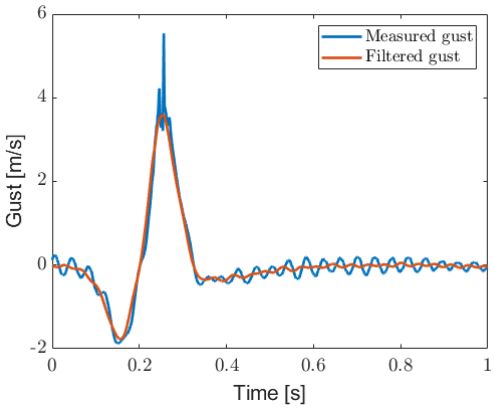

Fig. 5 *Measured gust and filtered gust*

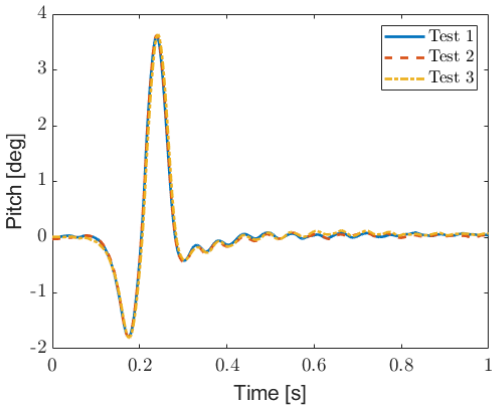

Fig. 6 *Discrete gust, evaluation repeatability*

or gust frequency gives consistent results. Figure 7 shows that varying airspeed, and gust frequency only give consistent results for small (5° and 10°) pitch amplitude. The gust profile is chaotic and inconsistent for low gust frequency and high maximum vane rotation amplitude, the gust profile is chaotic and inconsistent.

It is likely that the behavior is related to dynamic stall. This phenomenon is significantly affected by the reduced frequency, while the Reynolds number has only a small effect on it [35, 36]. The effect of reduced frequency on the dynamic stall phenomenon is a well-studied problem; in particular, the dynamic stall angle increases with reduced frequency [35–38]. In the case of reduced frequencies smaller than 0.05, it is possible to consider the flow as steady flow, while for reduced frequencies greater than 0.2, the flow is highly unsteady [38]. The results shown in Figure 7 cover a wide range of reduced frequencies. In the literature for a profile NACA0015 at Reynolds number $3.6 \cdot 10^5$ the static stall angle is at 13.9° [39]. In the case of airspeed 26 m/s and gust frequency 1 Hz, the reduced frequency is 0.024, and the Reynolds number is $2.45 \cdot 10^5$, so, it is plausible that at 15° the profile is stalled and at 20° the profile is well beyond the stall condition. At the same gust frequency and lower airspeed, the reduced frequency is increasing, so the effect of the dynamic stall vortex is becoming more important. The low repeatability of the measurements affected by the dynamic stall is expected because experimental data has shown that the stall behavior is associated with different separation patterns and is not repeatable [40, 41]. Similar trends are exhibit for gusts with higher frequencies. Based on the repeatability and shape of the gust, for the very low value of k, the gust generator can always generate gusts for the vane rotation amplitude of 5°. For $k \geq 0.19$, it can create gusts for vane rotation amplitude of 10° and 15° and for $k \geq 0.38$, it can create gusts for vane rotation amplitude of 20°. The results are also in agreement with previous similar work [19].

The gusts in Figure 8 for gust frequencies greater than 10 Hz show some oscillations at 19.7 Hz, after the main peak, which is due to vibrations of the vanes. This effect is not important in harmonic excitation because the transient response has decayed in the steady state, so that the gust is at the same frequency as the vane rotation.

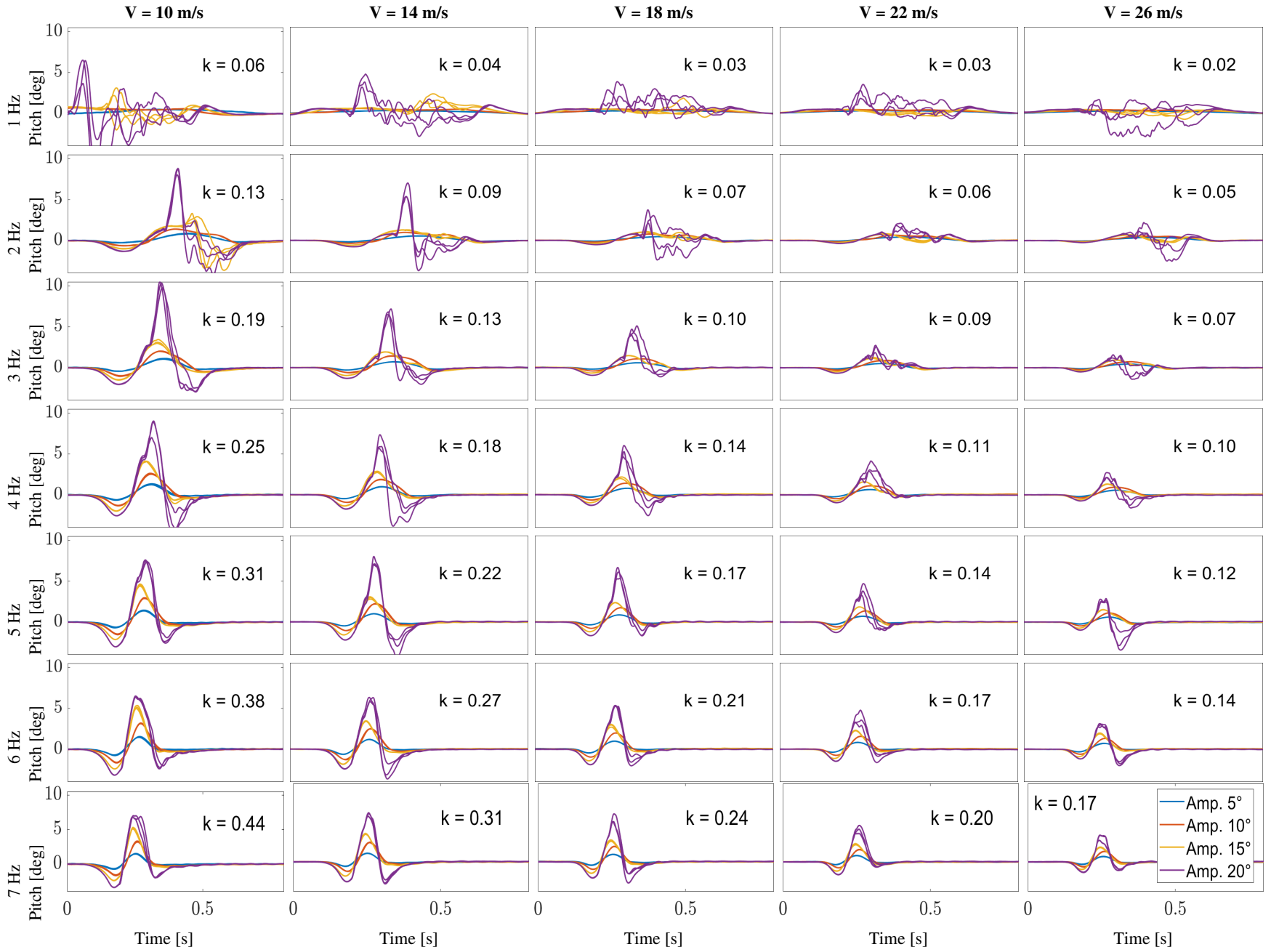

Fig. 7 *Discrete gust vane rotations amplitude of* 5°, 10°, 15° *and* 20°, 1 *to* 7 *Hz rotation frequency. Each case was repeated three time and all data are plotted*

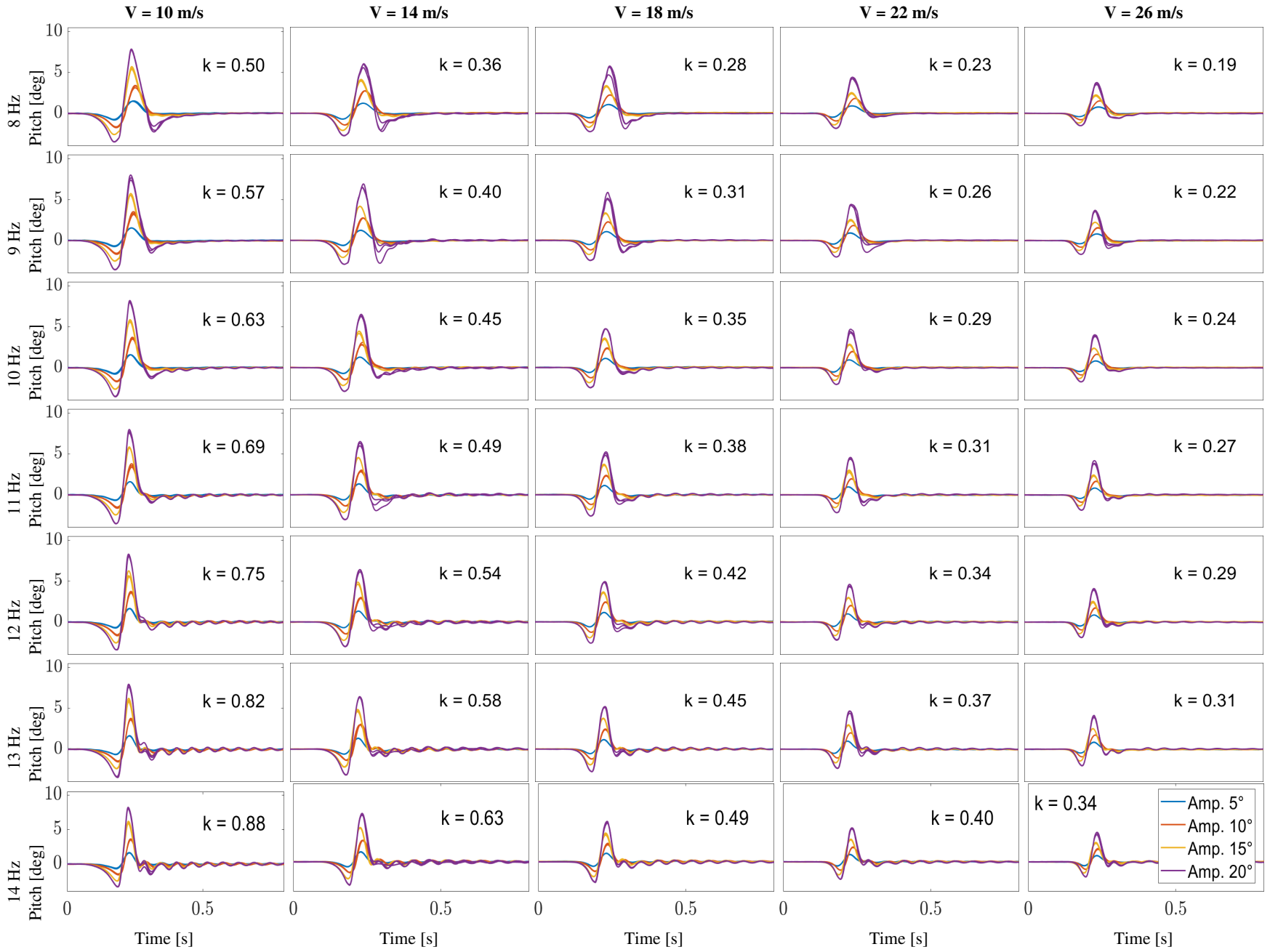

Fig. 8 *Discrete gust vane rotations amplitude of* 5°, 10°, 15° *and* 20°, 8 *to* 14 *Hz rotation frequency. Each case was repeated three time and all data are plotted*

Figure 9 shows the maximum gust peaks as a function of frequency and maximum vane angle of rotation generated using Eq. 3 at an airspeed of 18 m/s. At each frequency considered, the trend is again linear in the range of 5° to 15°. For frequencies greater than 9 Hz, the trend is linear in the range 5° to 20°. Similar trends have been observed at airspeeds of 10 m/s, 14 m/s, 22 m/s, and 26 m/s.

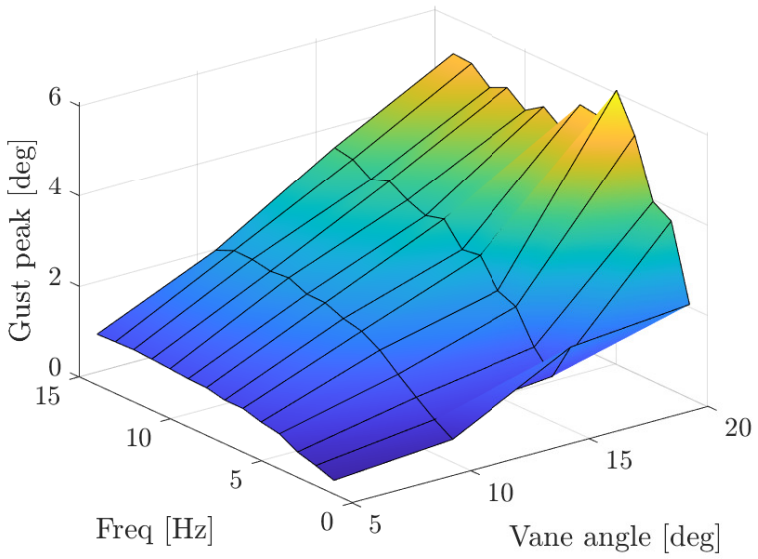

Fig. 9 *Maximum gust peaks as a function of frequency and maximum vane angle of rotation for gusts at* 18 *m/s*

B. Continuous sinusoidal gusts

Figures 10 and 11 show the pitch angle measurements in the case of the continuous gust. As in the case of the discrete gust, increasing the airspeed, causes the maximum peak to reduce while increasing the pitching frequency of rotation or increasing the maximum vane rotation amplitude causes the peak to increase.

C. Flow uniformity

Two tests were performed to assess the uniformity of the gust produced by the gust generator in the wind tunnel cross-section. In both cases, the symmetry of the test chamber is considered. In the first test, the anemometer was moved horizontally (in the vane span direction) in three additional positions with respect to the central position. Each point is 150 mm from the previous one. Figure 12a shows the locations considered. Figure 12b shows the discrete gusts measured at the four positions, considering an airspeed of 10 m/s, 10° maximum vane rotation, and a gust frequency range of 5 Hz to 10 Hz. The results show a good uniformity of the gust field at all the stations considered. For all the cases considered, the difference between the gusts peaks measured at the central position and the ones measured at positions 2, 3, and 4 are 0.046°, 0.003°, and 0.163°, respectively. The uniformity of the flow ensures that in future aeroelastic tests, the wing will be subjected to a uniform gust along the span.

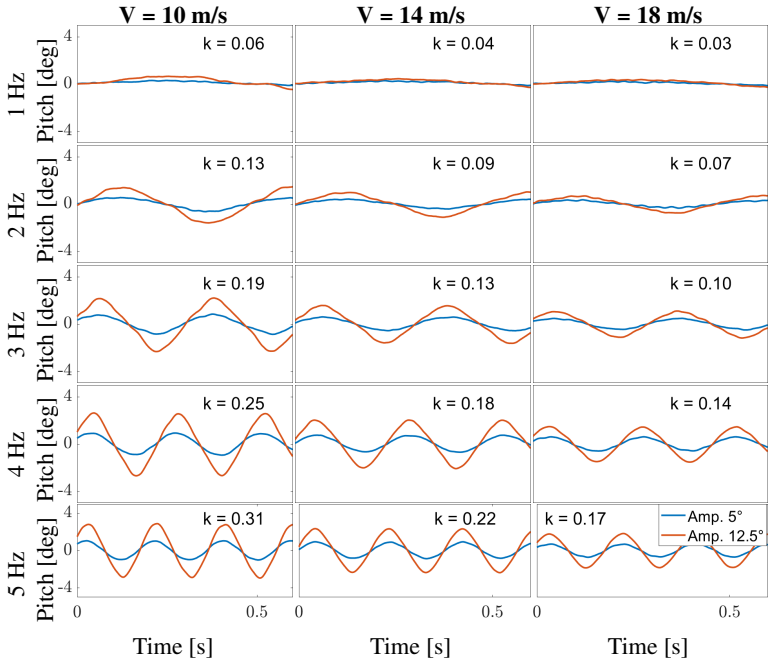

Fig. 10 *Continuous gust for vane rotations amplitude of* 5° *and* 12.5°*, at* 1 *to* 5 *Hz*

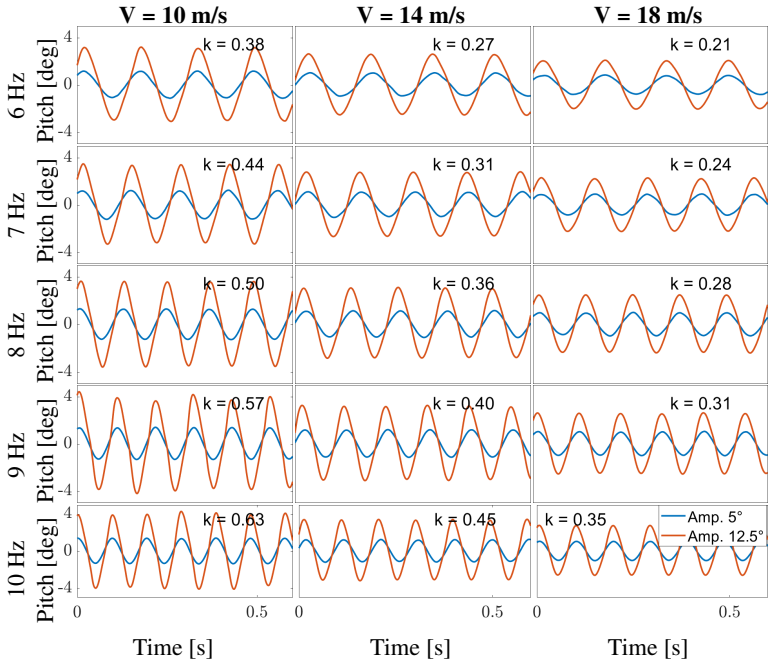

Fig. 11 *Continuous gust for vane rotations amplitude of* 5° *and* 12.5°*, at* 6 *to* 10 *Hz*

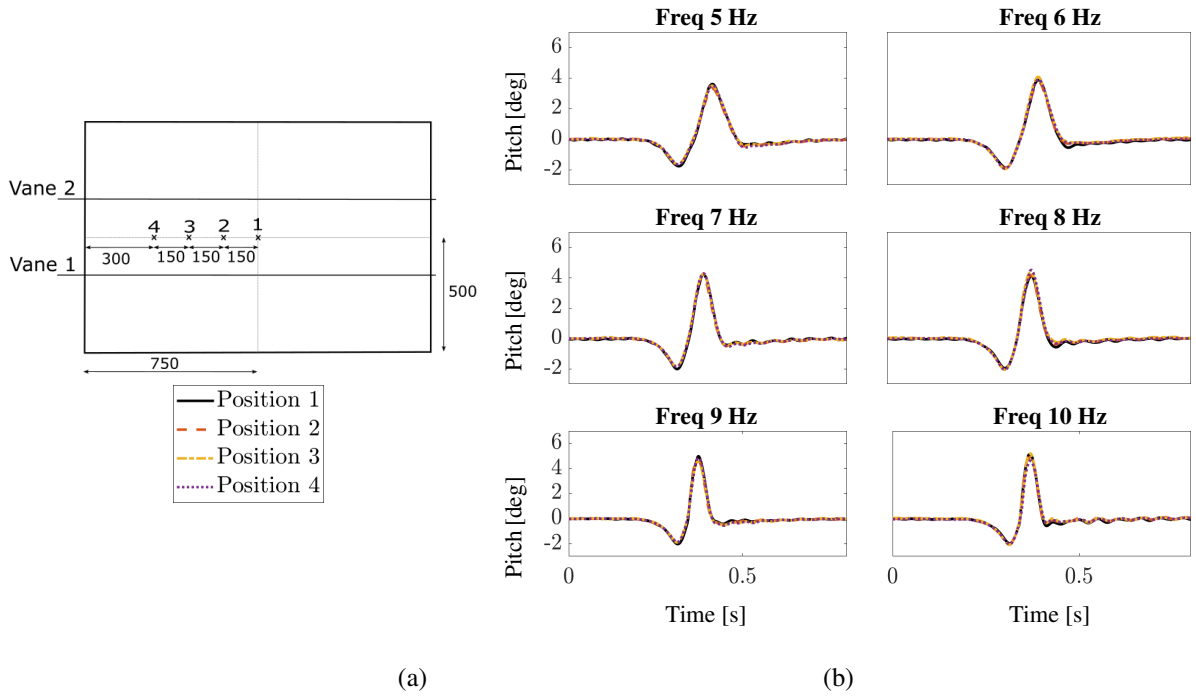

Fig. 12 *Gust uniformity at different horizontal locations* (a) *and discrete gusts at each location* (b)

In the second test, five points in the vertical direction spaced at an equal distance were considered. Figure 13a shows the locations considered. Positions 1 and 2 are between the vanes, position 3 is on the wake of the vane, and positions 4 and 5 are between the vane and the wind tunnel top wall. Figure 13b shows the discrete gust measured at the different locations, considering an airspeed of 10 m/s, 10° maximum vane rotation, and gust frequencies in the range from 5 Hz to 10 Hz. The results show a slight difference between the gust measured at position 1 and position 2. The measurements show a similar trend at each frequency and at all the positions considered with the maximum peak reducing from position 1 to position 5. Midway between the two vanes, the gust has its maximum value due to the contribution of both vanes, whereas moving towards a vane, the effect of the farthest vane is reduced. Position 3 is in the wake of the vane, and as such it is characterized by high fluctuations before and after the gust.

V. Improvement of the '1-cos' gust profile

The measurements of the discrete gust described in Figures 5 to 8, 12, and 13 show a negative peak before and after the positive peak. This behaviour can be observed in the measurements from other gust generator tests [19, 20, 27], but there are no published methods to counter this undesirable effect effectively. The negative peak before the gust is due to the starting vortex that is generated in the wake of the pitching vanes as their angle of attack with respect to the free stream increases [42]. Similarly, the negative peak after the gust is due to the stopping vortex [43].

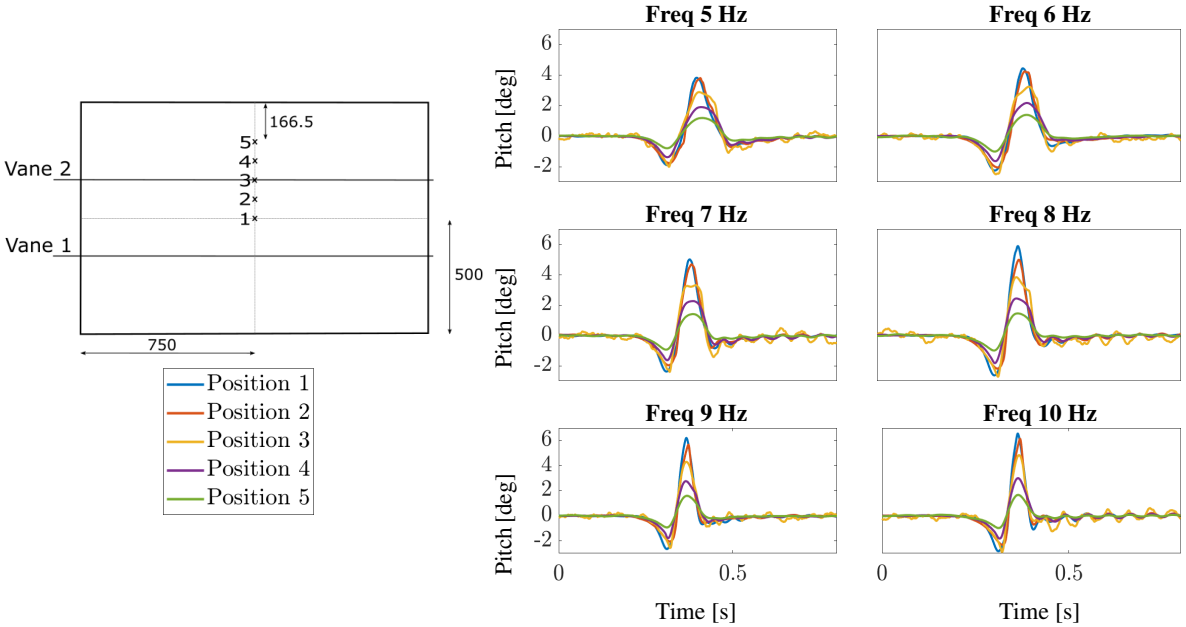

(a) (b)

Fig. 13 *Gust uniformity at different vertical locations* (a) *and discrete gusts at each location* (b)

To improve the '1-cos' gust, two test campaigns have been performed. The first test campaign aimed to identify a transfer function that links the gust time history with the motor rotation and hence to find the motor rotation required to obtain an improved '1-cos' gust. A parametric study of the vane rotation has been performed in the second test campaign. To quantify the effect of different techniques on the alleviation of the negative peaks, a Negative Peak Factor (NPF) n has been defined as

$$n = \left| \frac{\alpha_{min}}{\alpha_{max}} \right| \tag{7}$$

where α_{min} and α_{max} correspond to the minimum and maximum values of the gust, respectively.

A. Identification and results of the transfer function

The Navier-Stokes equations, which describe the motion of fluids, are notoriously non-linear [44]; nevertheless, as a first approximation, we considered approximating the gust generator in the wind tunnel as a linear system. The input-output relation for a linear system is described by a transfer function. To experimentally identify the transfer function, the measurements from the cross hot-wire sensor and an encoder on the motor have been recorded on the same National Instruments data acquisition system. Two strategies have been considered, a series of periodic sinusoidal rotations and impulsive rotation of the vanes.

1. Periodic sinusoidal vane rotation

In the first case, the vane rotation has been obtained from Eq.(5) for $A = 10°$ and values of f from 1 Hz to 10 Hz in 1 Hz increments. Figure 14 shows the vane rotation and the measured angle of attack at 18 m/s. It is possible to calculate the input-output relation in terms of amplitude and phase for each continuous sinusoidal rotation. To identify the transfer function, an optimisation process based on a genetic algorithm has been used. Figure 15 shows the experimental points obtained and the identified transfer function at 18 m/s.

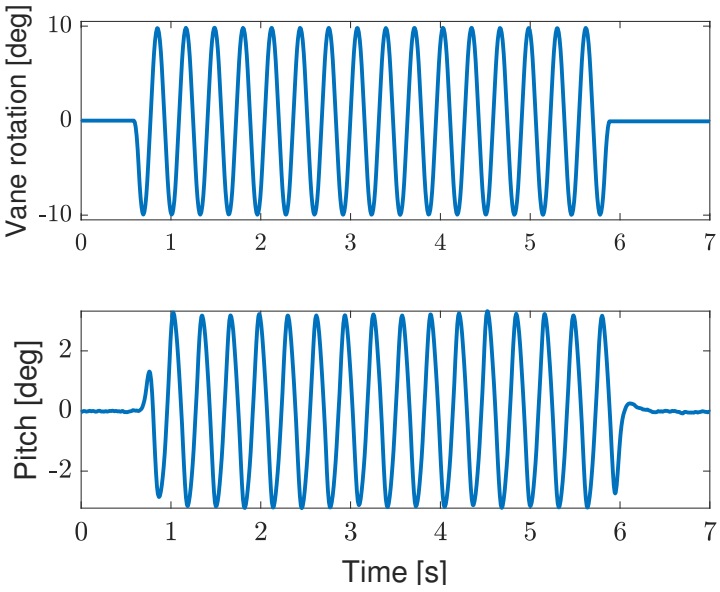

Fig. 14 *Vane rotation and gust measured by the cross hot-wire sensor at* 18 *m/s*

The amplitude of the experimental points suggests a behavior as a first-order system with a zero at a lower frequency with respect to the pole. The phase of the experimental points suggests a pure delay. Although the identification of the transfer function should consider amplitude and phase together, in this work, amplitude and phase identification has been performed separately. This strategy was followed because the objective of this work was to find a simplified input-output relation based on the experimental results, while future works will consider more sophisticated identification strategies. The procedure has been repeated at 10 m/s and 14 m/s. The results found have similar trends as the one in Figure 15. For each airspeed, a first-order transfer function of the type

$$H_1(s) = K\frac{s+z}{s+p} \tag{8}$$

has been identified from the experimental points of the amplitude. K, z, and p are the gain factor, zero, and pole of the transfer function, respectively. For each airspeed, from the experimental points of the phase, it has been identified a pure

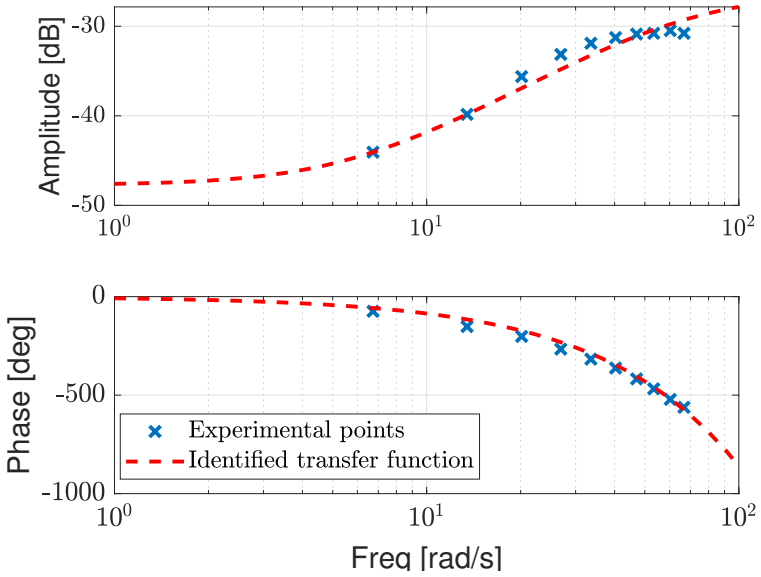

Fig. 15 *Identified transfer function from sinusoidal test at* 18 *m/s*

delay transfer function of the type

$$H_2(s) = e^{-\tau s} \tag{9}$$

where τ is the delay of the transfer function. Table 3 shows K, z, p, and τ. The identified delay, τ, represents the time

Airspeed [m/s]	K [-]	z [rad/s]	p [rad/s]	Identified delay τ [s]	Convection time t_{conv} [s]	Shedding time t_{s} [s]
10	0.0535	0.0001	30.67	0.157	0.123	0.034
14	0.0470	0.00003	39.33	0.123	0.088	0.035
18	0.0495	5.81	69.9	0.105	0.068	0.037

Table 3 *Identified delay, convection time, and shedding time at* 10 *m/s,* 14 *m/s, and* 18 *m/s identified from continuous sinusoidal vane rotation*

between an ideal impulse vane rotation and the measured gust. Further to the transfer function parameters, Table 3 also shows the convection time, t_{conv}, and the shedding time, t_{s}. The convection time is defined as

$$t_{\text{conv}} = \frac{d_{\text{vs}}}{V_\infty} \tag{10}$$

where d_{vs} is the longitudinal distance between the vane trailing edge and the sensor location. The shedding time is defined here as

$$t_{\text{s}} = \tau - t_{\text{conv}} \tag{11}$$

In the airspeed range considered, the shedding time is practically constant.

Further to the shedding time for an ideal gust impulse, the shedding time for realistic vane rotations is considered next. At each airspeed and frequency of the vane continuous sinusoidal rotation the sinusoidal excitation shedding time t_{ss}, has been calculated as

$$t_{ss} = \tau_f - t_{\text{conv}} \tag{12}$$

where τ_f is the time delay between the sinusoidal vane rotation and the measured gust, as measured in the experiments. Figure 16 shows the sinusoidal excitation shedding time at 10 m/s, 14 m/s, and 18 m/s, and the identified shedding time as a function of the vane frequency sinusoidal rotation. The sinusoidal excitation shedding time shows a similar trend for all airspeeds, decreasing with increasing vane rotation. A second-order polynomial equation, t_{ss}^{i}, has been fitted to the experimental data to identify the sinusoidal rotation shedding time t_{ss} as a function of the frequency of the vane rotation f as

$$t_{\text{ss}}^{\text{i}} = 0.0002f^2 - 0.0063f + 0.07 \tag{13}$$

It is noted that for the highest vane rotation frequency, the mean shedding time is 0.031 s, very close to the relevant identified value for the ideal gust.

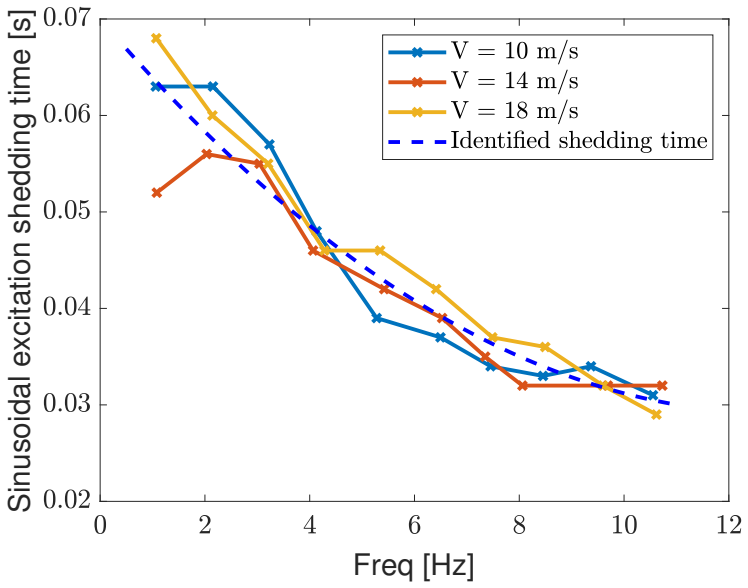

Fig. 16 *Experimental and identified shedding times from continuous sinusoidal vane rotation*

2. Impulsive vane rotation

In the second case, a series of impulse rotations have been considered by using Eq. (3) at $A = 5°$, for increasing values of f and airspeed of 10 m/s, 14 m/s, and 18 m/s. From each vane rotation and gust time history, a transfer function has been calculated and the mean of all the calculated transfer functions has been used to identify the transfer function.

As in the case of continuous sinusoidal vane rotation, the amplitude of the transfer function suggests a first-order system while the phase suggests a pure delay. The coefficients of the transfer functions $H_1(s)$ and $H_2(s)$, see Eqs. 8 and 9, have been identified. Figure 17 shows the experimental points, the average transfer function and the identified transfer function at 18 m/s. Table 4 shows for each airspeed the transfer function parameters along with convection time, and shedding time identified from the measurements. The identified delays in Tables 3 and 4 have a maximum difference of

Airspeed [m/s]	K [-]	z [rad/s]	p [rad/s]	Identified delay τ [s]	Convection time t_{conv} [s]	Shedding time t_{s} [s]
10	0.0461	2.18	23.85	0.159	0.123	0.036
14	0.0503	4.77	45.16	0.127	0.088	0.039
18	0.0370	6.76	42.55	0.109	0.068	0.041

Table 4 *Identified delay, convection time, and shedding time at* 10 *m/s,* 14 *m/s, and* 18 *m/s identified from impulse vane rotation*

0.004 s, which is considered negligible since the sampling frequency was 1 kHz.

3. Results of the identified transfer functions

Figure 18 shows the identified transfer functions at 18 m/s in the two cases considered, and they have a similar trend. In the frequencies of interest, the amplitude of the transfer function increases with the frequency, as observed

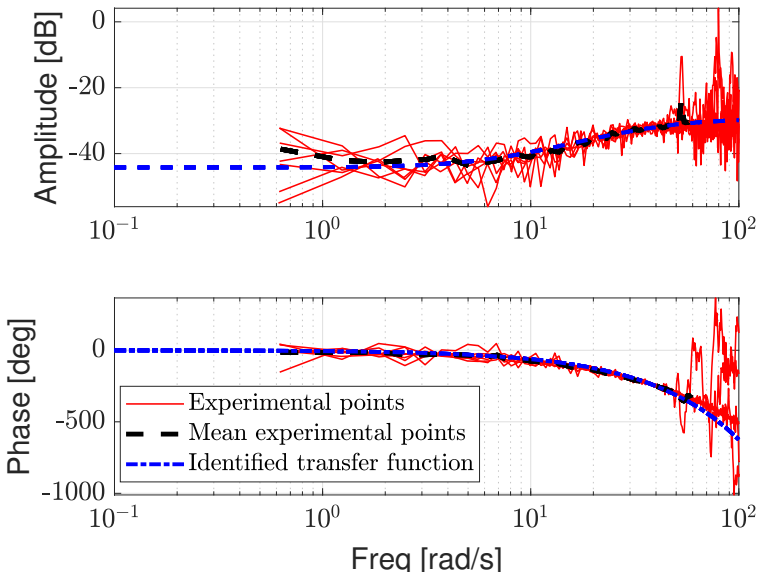

Fig. 17 *Measured transfer function, mean transfer function and identified transfer function from impulse tests at* 18 *m/s*

from Figures 7 to 13. The phase increases with the frequency in accordance with the Theodorsen function [45]. Figure 2 shows that discrete '1-cos' gusts are characterized by significant low-frequency components and so a good characterisation of the low frequency response is required. Although the identified transfer functions have analogous

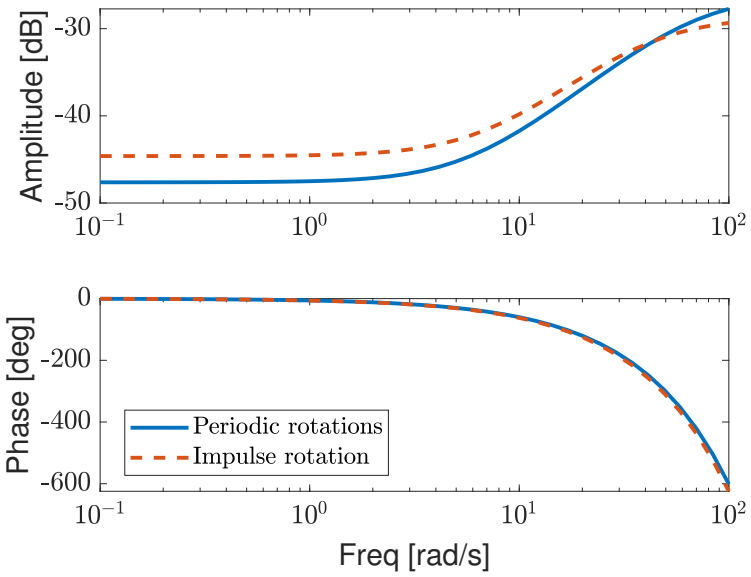

Fig. 18 *Comparison of identified transfer functions at* 18 *m/s*

trends both in terms of amplitude and phase, the continuous sinusoidal rotations do not provide a good characterisation of the low frequency range because gust at low frequencies are associated with low amplitude. Indeed, the gust generator cannot produce continuous gusts for frequencies lower than 1 Hz. At the same time, higher amplitude, low-frequency content is provided in the case of impulse rotation of the vane. It hence decided only to consider the transfer function obtained by impulse vane rotation at 18 m/s for the remaining of this work.

To calculate the vane rotation required to obtain a '1-cos' gust as in Eq. (1) and in Figure 1 the desired gust and the vane rotation has been considered in the frequency domain. The vane rotation amplitude and the phase content have been considered separately. The amplitude has been calculated at each frequency by multiplying the inverse of the amplitude of $H_1(j\omega)$ by the corresponding amplitude of the desired gust. The phase has been calculated at each frequency by multiplying the inverse of $H_2(j\omega)$ by the corresponding phase of the desired gust. The generated vane rotation has been applied at the gust generator vanes. Figures 19 and 20 show the results obtained in the case of desired maximum amplitudes of 1°, 2°, and 3° and gust frequencies between 6 to 15 Hz and the desired gust. The results show an attenuation of the negative peaks. However, compared to the desired gust, it is noted that deviations from the ideal '1-cos' persist.

A direct comparison between the gusts obtained considering vane rotations from Eq. (3), and the inverse of the transfer function is possible only when the same vane pitch amplitude produces similar gusts. Indeed, Eq. (3) does not contain any previous knowledge of the expected maximum gust amplitude. In the following, a comparison is given between similar gusts obtained by '1-cos' vane rotation and by the inverse of $H_1(s)$ and $H_2(s)$. The comparison aims to compare similar gusts obtained with different strategies, although the two strategies followed two different aims. Indeed,

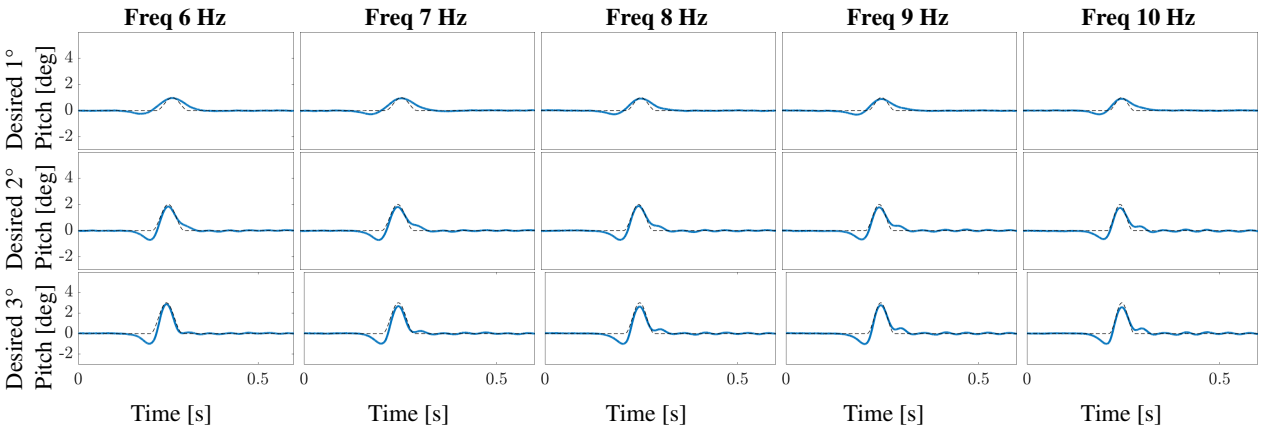

Fig. 19 *Discrete gust vane rotations with desired AoA* 1°, 2° *and* 3°, *and frequency* 6 *to* 10 *Hz and ideal '*1*-cos' gust at* 18 *m/s* (*black dashed line*)

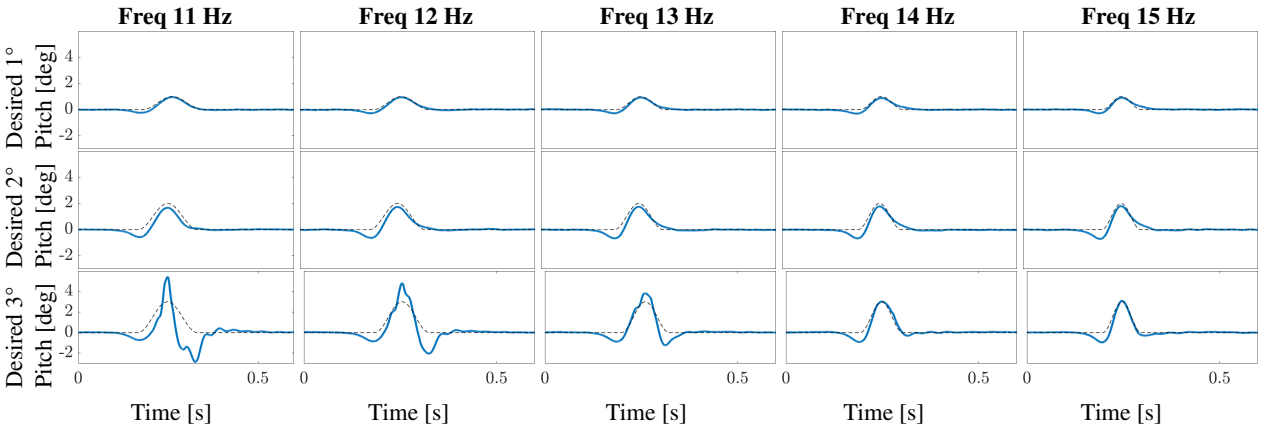

Fig. 20 *Discrete gust vane rotations with desired AoA* 1°, 2° *and* 3°, *and frequency* 11 *to* 15 *Hz and ideal '*1*-cos' gust at* 18 *m/s* (*black dashed line*)

in the first case, the vane rotation was imposed without any knowledge of the desired gust, while in the second case, the vane rotation was calculated to obtain the desired gust. As an example, the case with a gust of maximum amplitude of ∼3° at 9 Hz is considered. In order to achieve such a gust, a '1-cos' vane rotation of 15° at the same frequency is required. The motor rotation found by the inverse of $H_1(s)$ and $H_2(s)$ for a desired discrete gust with a maximum amplitude of 3° is shown in Fig. 21. Figure 22 shows the desired discrete gust with a maximum amplitude of 3° and frequency of 9 Hz, the gust produced by a '1-cos' vane rotation of amplitude 15° and the gust produced using the vane rotation found using the inverse of the transfer function identified. The proposed method allows the attenuation of both the negative peaks with direct control on the gust amplitude. The NPF for the gust produced by '1-cos' vane rotation is 0.53, while the NPF for the gust produced using the inverse of the transfer function is 0.30.

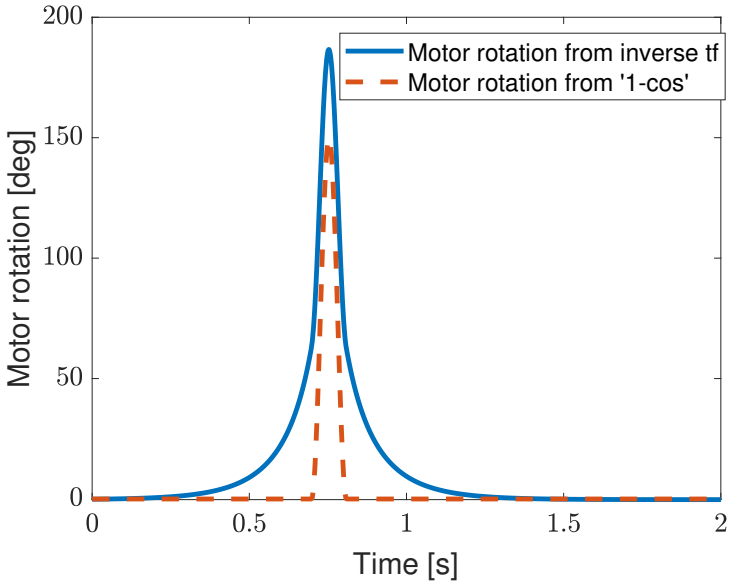

Fig. 21 *Comparison motor rotation found from inverse transfer function and '1-cos'*

B. Results of the parametric study

The vane rotation defined in Eq. (3) has a zero slope at $t = 0$, and for $t > 0$ the slope increases and decreases rapidly before the vanes attain their maximum value (due to $\frac{d}{dt}(1 - \cos(t)) = \sin(t)$). In the same way, at $t = 0.5/f$ and at $t = 1/f$ the slope is zero and between these points the slope decreases and increases quickly. As previously discussed, the negative peaks in the discrete gusts are due to the starting and the stopping vortices and their intensity is related to the rate of change of lift, or equivalently the angle of attack. Considering Eq. (3) as a reference, a parametric study has been performed on the definition of the vane rotation to attenuate these vortices. The parametric study performed at 18 m/s, has shown a reduction of both negative peaks when Eq. (3) is combined with a growing exponential curve for

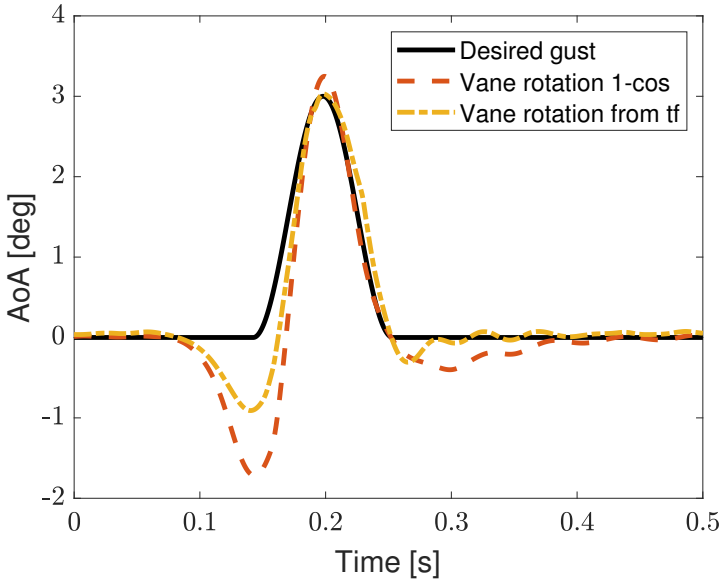

Fig. 22 *Comparison desired gust profile at 9 Hz, gust obtained from '1-cos' vane rotation and gust obtained from motor rotation obtained from the inverse transfer function*

$t < 0.5/f$ and a decaying exponential curve for $t > 0.5/f$. It has been shown that defining the vane rotation as

$$\theta(t) = \begin{cases} \exp(Bt) - 1 & \text{for} \quad 0 \le t < t_1 \\ \frac{A}{2}\left[1 - \cos(2\pi f(t - t_{01}))\right] & \text{for} \quad t_1 \le t \le t_2 \\ \exp(C(t - t_{02})) & \text{for} \quad t > t_2 \end{cases} \tag{14}$$

can reduce the NPF and produce accurate discrete gusts. To determine the seven unknowns of Eq. (14) (A, $B, C, t_{01}, t_{02}, t_1, t_2$) the parameters of Table 5 have been used for four values of A. The values of t_1 and t_2 can be found

	$A = 5°$	$A = 10°$	$A = 15°$	$A = 20°$
t_{01}	0.15 s	0.20 s	0.25 s	0.30 s
t_3	$t_{01} + 4/f$	$t_{01} + 4/f$	$t_{01} + 4/f$	$t_{01} + 4/f$
$\theta(t_1)$	0.9A	0.9A	0.9A	0.9A
$\theta(t_2)$	0.5A	0.5A	0.5A	0.5A
$\theta(t_3)$	0.003°	0.003°	0.003°	0.003°

Table 5 *Selected parameters*

considering $\theta(t_1) = 0.9A$ in the first half of the cosine period and $\theta(t_2) = 0.5A$ in the second half of the cosine period. From $\theta(t_1) = 0.9A$, t_1 can be found. Imposing the continuity at $\theta(t_1)$ the coefficient B can be found. Imposing the continuity at $\theta(t_2)$ and the point $\theta(t_3)$ the coefficients C and t_{02} can be found. Figure 23 shows the vane rotation in the case of Eq. (3) where an offset of t_{01} has been added to the cosine function and in the case of Eq. (14) where the three

constraint points used are shown.

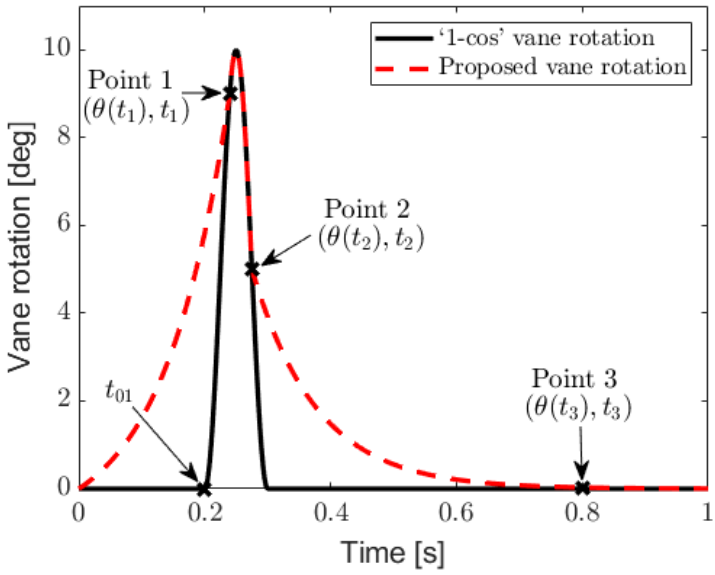

Fig. 23 *Proposed method to parameterize the vane rotation*

The effect of the parameters shown in Table 5 on the identified gust profile is worth investigating. Figures 24, 25 and 26 show the effect of t_{01}, $\theta(t_2)$ and t_3 on the gust produced. The selection of t_{01} affects the behavior of the first part of the gust because it controls the starting vortex. Indeed, a small value of t_{01} creates a negative peak before the gust similar to that of the '1-cos' vane rotation while a high value of t_{01} creates a positive peak. The selection of t_{01} has an impact on the maximum peak of the gust produced; a faster vane rotation creates a gust with a higher maximum peak. Experiments suggest the use of a value of t_{01} proportional to the maximum vane rotation amplitude. $\theta(t_2)$ and t_3 control the second part of the gust, the negative peak due to the stopping vortex, and the hump in the last part of the gust. A small value of $\theta(t_2)$ produces a negative peak after the gust and delays the creation of the hump. $\theta(t_2)$ affects the maximum peak of the gust produced; a small value of $\theta(t_2)$ creates a gust with a higher maximum peak. $\theta(t_2)$ has been kept constant for all the cases considered. A small value of t_3 produces a negative peak after the gust and reduces the amplitude of the hump. t_3 has a negligible effect on the maximum gust peak. $\theta(t_1)$ has been kept constant because the effect of the starting vortex is controlled by t_{01}. $\theta(t_3)$ has been kept at 0.003° which practically is equivalent to zero.

Figure 27 shows the gusts measured when Eq. (14) is used considering different maximum vane rotations A. The reduced frequencies k are in the range of 0.14 to 0.52. Based on the shape of the gust, the proposed method can create discrete gust for all values of k for vane rotation amplitudes of 5°, 10° and 15°, while for $k \geq 0.28$ it can create discrete gust for vane rotation amplitude of 20°. For maximum vane rotations of 5°, 10° and 15°, the results show a general reduction of the negative peaks. For high gust frequency, the results show that after the main peak, some oscillations due to the vane vibrations appear.

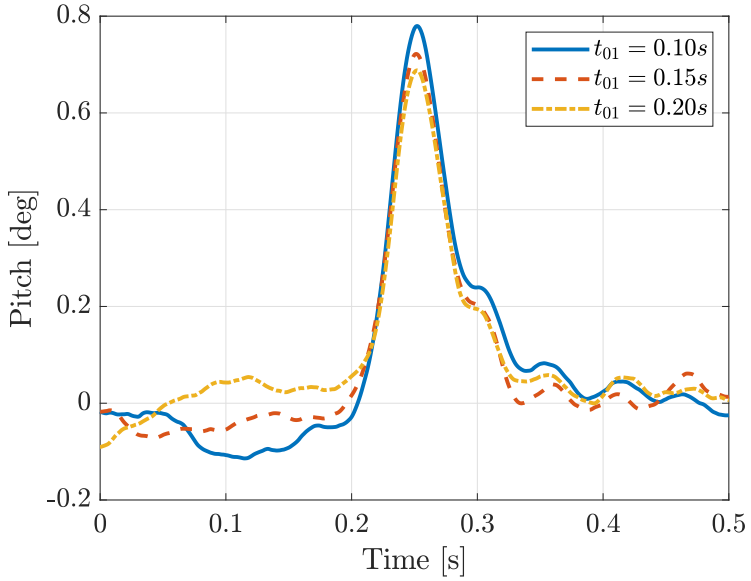

Fig. 24 *Proposed method, effect of t_{01} on the gust produced*

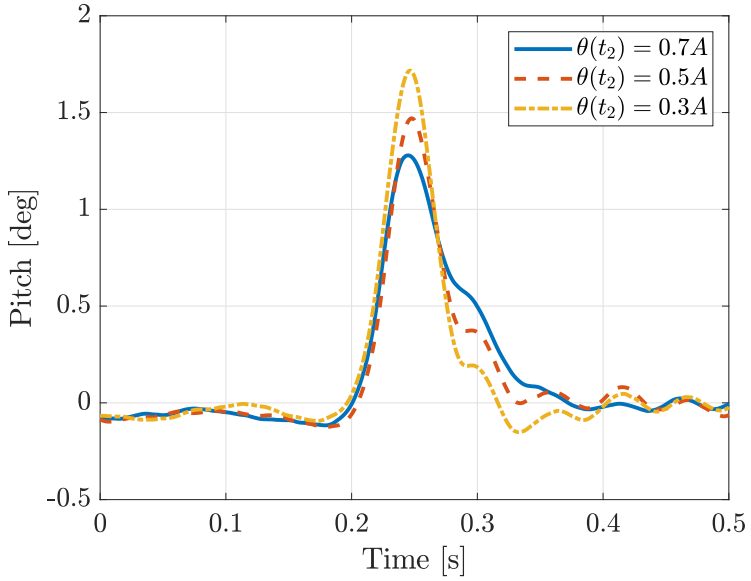

Fig. 25 *Proposed method, effect of $\theta(t_2)$ on the gust produced*

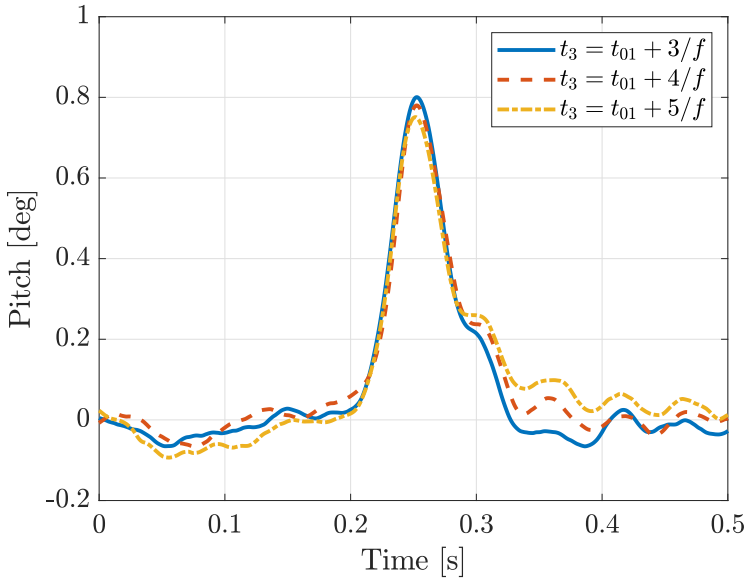

Fig. 26 *Proposed method, effect of t_3 on the gust produced*

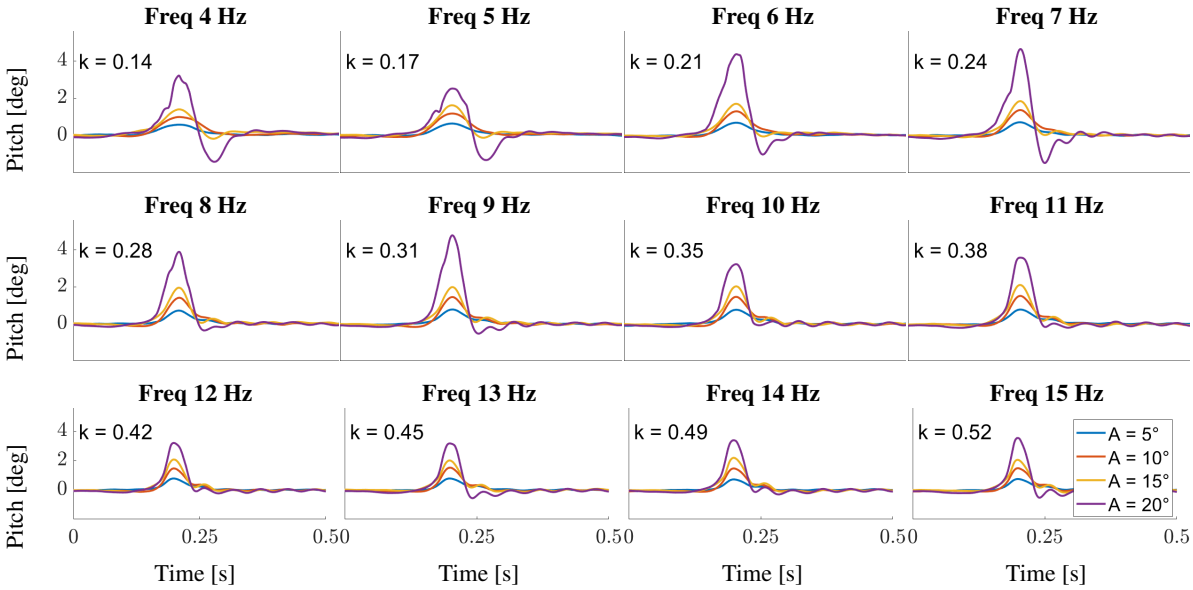

Fig. 27 *Proposed method to parameterize the discrete gust vane rotation for amplitude of* 5°, 10°, 15° *and* 20°, *and frequencies of* 4 *to* 15 *Hz*

The reduction of the negative peaks improves the frequency content of the gust. Indeed, Figures 28 and 29 show the frequency content of the measured discrete gusts at 18 m/s, frequency of 13 Hz, vane rotation for the amplitude of 5°, 10°, 15° and 20° in the case of '1-cos' vane rotation and the proposed method, respectively. Figures 28 and 29 also show the frequency content of discrete gusts with the same gust wavelength and maximum amplitude. The proposed method is able to produce discrete gusts with a more constant low-frequency content with respect to gusts produced by '1-cos' vane rotation.

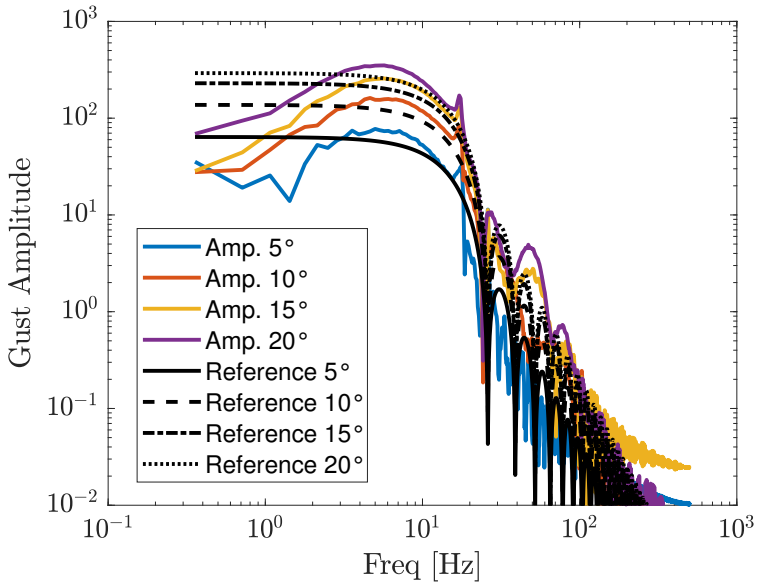

Fig. 28 *Frequency content of discrete gusts obtained at* 18 *m/s, frequency of* 13 *Hz, by '*1*-cos' vane rotation for amplitude of* 5°*,* 10°*,* 15° *and* 20° (*color lines*) *and frequency content of the equivalent exact discrete gusts with the same gust wavelength and maximum amplitude* (*black lines*)

A comparison between gusts produced by different vane rotations is provided here. Figure 30 shows the comparison between discrete gusts at 8 Hz generated by '1-cos' vane rotation and vane amplitude of 10°, from the vane rotation calculated from the inverse of the transfer function with the desired gust of 2° and the proposed method with $A = 15°$. Figure 30 also shows the corresponding ideal '1-cos' gusts. In the three cases considered, the mean square error is 0.16 in the case of the gust obtained by '1-cos' vane rotation, 0.029 for the gust obtained by the vane rotation from the inverse of the transfer function, and 0.0063 for the gust obtained by the vane rotation from the proposed method.

Figure 31 shows the maximum gust peaks as a function of frequency and maximum vane angle of rotation found using Eq. (14). At each frequency considered, the trend is linear in the range of 5° to 15°. In the linear region, Figure 31 can be used to calculate the maximum vane angle of rotation required to obtain the desired discrete gust. The proposed method results in gusts with lower amplitude compared with the maximum peak obtained by '1-cos' vane rotation (see Figure 9) for the same rotation angle and frequency. Indeed, Figures 24, 25 and 26 show the effect of the introduced parameters in attenuating the maximum gust peak.

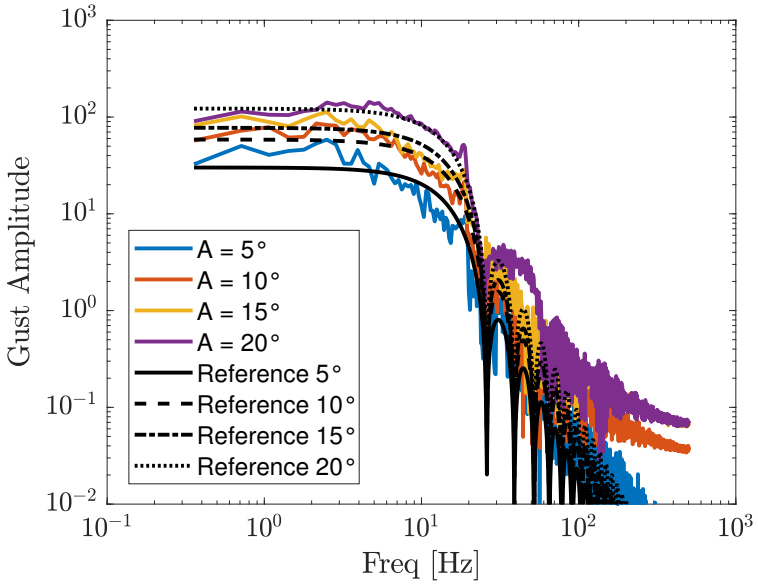

Fig. 29 *Frequency content of discrete gusts obtained at* 18 *m/s, frequency of* 13 *Hz, by the proposed method for amplitude of* 5°, 10°, 15° *and* 20° (*color lines*) *and frequency content of the equivalent exact discrete gusts with the same gust wavelength and maximum amplitude* (*black lines*)

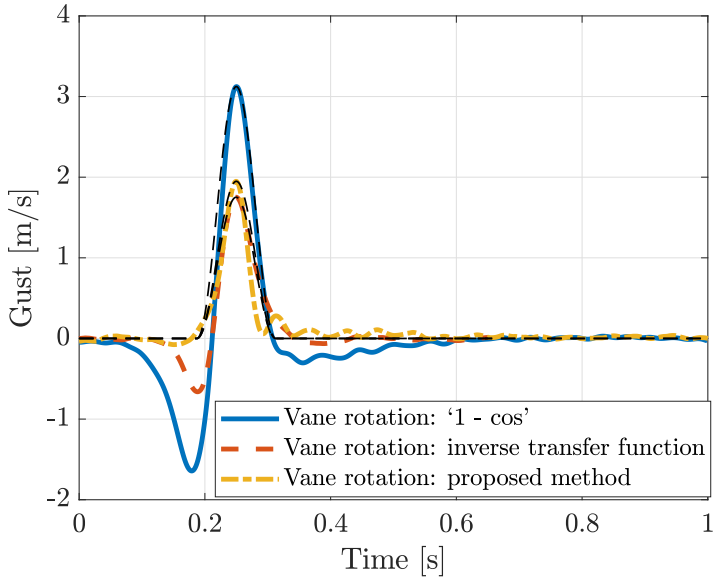

Fig. 30 *Discrete gust at* 8 *Hz from* '1-*cos*' *vane rotation and vane amplitude* 10°, *from the vane rotation calculated from the inverse of the transfer function with a desired gust of* 2°, *from the proposed method with* $A = 15°$ *and corresponding ideal* '1-*cos*' *gusts* (*black dashed lines*)

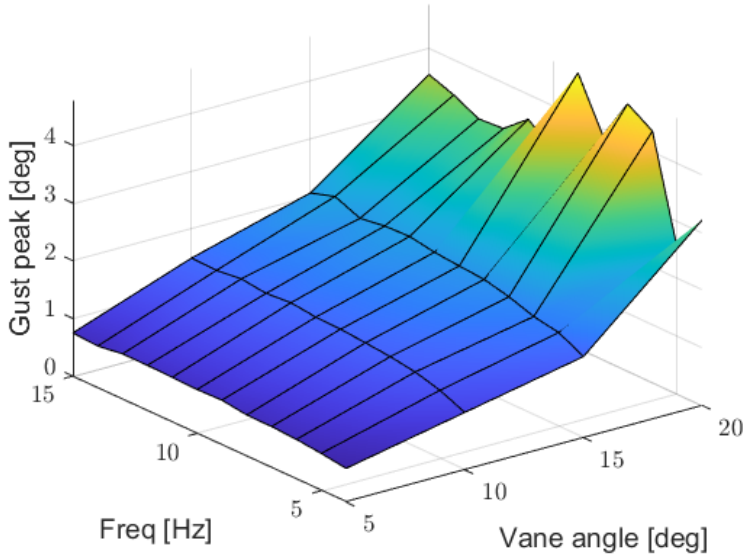

Fig. 31 *Maximum gust peaks as a function of frequency and maximum vane angle of rotation*

The three methods used to generate gusts are compared in terms of NPF. Figure 32 shows the NPF for discrete gust in the frequency range of 6 Hz to 14 Hz, in the case of '1 - cos' vane rotations, vane rotations from the inverse transfer functions and vane rotations from the proposed method. In the case of '1 - cos' vane rotations the mean NPF is 0.51 with its minimum for a vane rotation amplitude of 20° and a frequency 6 Hz due to the high amplitude of the positive peak. For gusts obtained from the vane rotations calculated from the inverse transfer functions, the mean NPF is 0.36. In this case, the maximum NPF is at low frequencies and the desired angle of attack of 3°, where the dynamic stall creates a chaotic behavior. The gusts produced by the vane rotations defined by the proposed method have a mean NPF of 0.06. The results show a constant NPF for all cases except for high vane rotation amplitude at low frequency due to the dynamic stall.

VI. Conclusions

A two vanes computer controlled gust generator has been designed and successfully implemented in the Swansea University wind tunnel. A literature review has been used as a guide for the design of the main components. Experimental data, collected from a cross hot-wire sensor, confirmed that the system is reliably capable of creating uniform discrete and continuous sinusoidal gusts. The results have shown good repeatability and agree with previous similar work. Discrete gusts have shown discrepancies between the desired and the measured gusts. A literature review on unsteady aerodynamics has suggested that dynamic stall, and the starting and stopping vortices are the primary reason behind this difference. Two techniques to improve the discrete gusts have been proposed. Transfer functions have been identified using periodic and impulsive vane oscillations and gave similar results. The transfer functions identified from impulsive

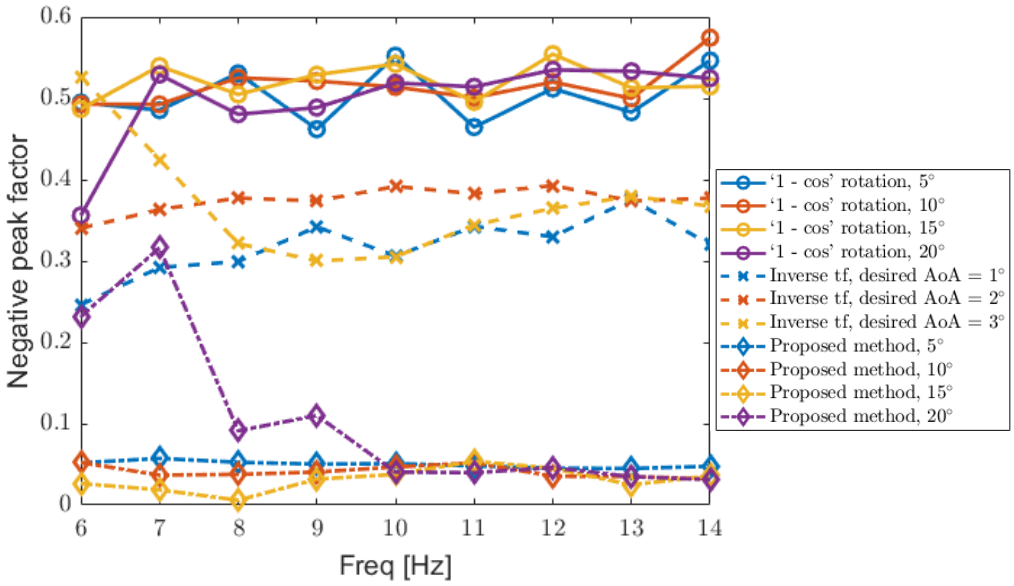

Fig. 32 *Negative peak factor using the three methods*

vanes oscillation have been used to calculate the vane rotation required to obtain an improved discrete gust. The results have shown a reduction of the negative peaks, although the high nonlinearity due to the unsteady aerodynamic effects has shown the limitation of this approach. The parametric study results have shown that using a more complicated vane rotation function, it is possible to obtain discrete gusts with negative peaks one order of magnitude smaller than with respect to the previous cases. The mean square error between the desired and measured gust is reduced by one order of magnitude when using the vane rotation from the inverse of the transfer function and two orders of magnitude when using the proposed method when compared to the '1-cos' vane rotation.

This work has shown that it is possible to create improved discrete gusts. Therefore, in future aeroelastic wind tunnel tests, the wing will be excited by gusts with a similar frequency content as the regulations require. The undesired effects of dynamic stall can be prevented by avoiding a high angle of attack at low reduced frequencies. For discrete gusts, undesired negative peaks related to the starting and stopping vortices can be attenuated by using appropriate vane rotations. The discrete gust frequency is limited by the structural vane vibration resonances and the maximum motor torque. Its first structural natural frequency should be kept as high as possible to avoid vane vibrations.

Acknowledgments

The research leading to these results has received funding from the Engineering Physical Science Research Council (EPSRC) through a program grant EP/R006768/1. Davide Balatti also acknowledges the PhD scholarship funded by the Faculty of Science and Engineering at Swansea University.

References

[1] Anderson, J. D., and Bowden, M. L., *Introduction to flight*, McGraw-Hill Higher Education, 2005.

[2] Fonte, F., Toffol, F., and Ricci, S., "Design of a wing tip device for active maneuver and gust load alleviation," *2018 AIAA/ASCE/AHS/ASC Structures, Structural Dynamics, and Materials Conference*, 2018, p. 1442. https://doi.org/10.2514/6.2018-1442.

[3] Ricci, S., De Gaspari, A., Riccobene, L., and Fonte, F., "Design and wind tunnel test validation of gust load alleviation systems," *58th AIAA/ASCE/AHS/ASC Structures, Structural Dynamics, and Materials Conference*, 2017, p. 1818. https://doi.org/doi.org/10.2514/6.2017-1818.

[4] Jutte, C. V., and Stanford, B. K., *Aeroelastic tailoring of transport aircraft wings: state-of-the-art and potential enabling technologies*, NASA/TM-2014-218252, 2014.

[5] Hargrove, W. J., *The C-5A active lift distribution control system*, NASA Technical Reports Server (NTRS) Accession No. 76–31148, 1976.

[6] Regan, C. D., and Jutte, C. V., *Survey of applications of active control technology for gust alleviation and new challenges for lighter-weight aircraft*, NASA/TM-2012-216008, 2012.

[7] Balatti, D., Khodaparast, H. H., Friswell, M. I., Manolesos, M., and Castrichini, A., "Aircraft turbulence and gust identification using simulated in-flight data," *Aerospace Science and Technology*, Vol. 115, 2021, p. 106805. https://doi.org/10.1016/j.ast.2021.106805.

[8] Barbarino, S., Bilgen, O., Ajaj, R. M., Friswell, M. I., and Inman, D. J., "A review of morphing aircraft," *Journal of intelligent material systems and structures*, Vol. 22, No. 9, 2011, pp. 823–877. https://doi.org/10.1177/1045389X11414084.

[9] Castrichini, A., Siddaramaiah, V. H., Calderon, D., Cooper, J., Wilson, T., and Lemmens, Y., "Preliminary investigation of use of flexible folding wing tips for static and dynamic load alleviation," *The Aeronautical Journal*, Vol. 121, No. 1235, 2017, pp. 73–94. https://doi.org/10.1017/aer.2016.108.

[10] Balatti, D., Khodaparast, H. H., Friswell, M. I., Manolesos, M., and Amoozgar, M., "The effect of folding wingtips on the worst-case gust loads of a simplified aircraft model," *Proceedings of the Institution of Mechanical Engineers, Part G: Journal of Aerospace Engineering*, 2021, p. 09544100211010915. https://doi.org/10.1177/09544100211010915.

[11] Cheung, R. C., Rezgui, D., Cooper, J. E., and Wilson, T., "Testing of Folding Wingtip for Gust Load Alleviation of Flexible High-Aspect-Ratio Wing," *Journal of Aircraft*, Vol. 57, No. 5, 2020, pp. 876–888. https://doi.org/10.2514/1.C035732.

[12] Wilson, T., Kirk, J., Hobday, J., and Castrichini, A., "Small scale flying demonstration of semi aeroelastic hinged wing tips," In Proceedings of the International Forum on Aeroelasticity and Structural Dynamics, Paper IFASD-2019-076, June 2019, pp. 1–19, 2019.

[13] Hesse, H., and Palacios, R., "Dynamic load alleviation in wake vortex encounters," *Journal of Guidance, Control, and Dynamics*, Vol. 39, No. 4, 2016, pp. 801–813. https://doi.org/10.2514/1.G000715.

[14] Karpel, M., Shousterman, A., Climent, H., and Reyes, M., *Dynamic Response to Wake Encounter*, 2013, p. 1921. https://doi.org/10.2514/6.2013-1921.

[15] Pereira, P., Almeida, L., Suleman, A., Bond, V., Canfield, R., and Blair, M., "Aeroelastic scaling and optimization of a joined-wing aircraft concept," *48th AIAA/ASME/ASCE/AHS/ASC Structures, Structural Dynamics, and Materials Conference*, 2007, p. 1889. https://doi.org/10.2514/6.2007-1889.

[16] Thomas, R. E., "PROGRESS REPORT GUST SIMULATION IN A WIND TUNNEL," Tech. rep., NASA CR-66235, 1966.

[17] Buell, D. A., "An experimental investigation of the velocity fluctuations behind oscillating vanes," Tech. rep., NASA-TN-D-5543, 1969.

[18] Lancelot, P. M., Sodja, J., Werter, N. P., and De Breuker, R., "Design and testing of a low subsonic wind tunnel gust generator," *Advances in aircraft and spacecraft science*, Vol. 4, No. 2, 2017, p. 125. https://doi.org/10.12989/aas.2017.4.2.125.

[19] Wood, K., Cheung, R., Richardson, T., Cooper, J., Darbyshire, O., and Warsop, C., "A New Gust Generator for a Low Speed Wind Tunnel: Design and Commissioning," *55th AIAA Aerospace Sciences Meeting*, 2017. https://doi.org/10.2514/6.2017-0502.

[20] Grissom, D., and Devenport, W., "Development and testing of a deterministic disturbance generator," 2004. https://doi.org/10.2514/6.2004-2956.

[21] Kuzmina, S., Ishmuratov, F., Zichenkov, M., and Chedrik, V., "Analytical-experimental study on using different control surfaces to alleviate dynamic loads," *47th AIAA/ASME/ASCE/AHS/ASC Structures, Structural Dynamics, and Materials Conference 14th AIAA/ASME/AHS Adaptive Structures Conference 7th*, 2006, p. 2164. https://doi.org/10.2514/6.2006-2164.

[22] Ricci, S., and Scotti, A., "Wind tunnel testing of an active controlled wing under gust excitation," *49th AIAA/ASME/ASCE/AHS/ASC Structures, Structural Dynamics, and Materials Conference, 16th AIAA/ASME/AHS Adaptive Structures Conference, 10th AIAA Non-Deterministic Approaches Conference, 9th AIAA Gossamer Spacecraft Forum, 4th AIAA Multidisciplinary Design Optimization Specialists Conference*, 2008, p. 1727. https://doi.org/10.2514/6.2008-1727.

[23] Neumann, J., and Mai, H., "Gust response: Simulation of an aeroelastic experiment by a fluid–structure interaction method," *Journal of Fluids and Structures*, Vol. 38, 2013, pp. 290–302. https://doi.org/10.1016/j.jfluidstructs.2012.12.007.

[24] Brion, V., Lepage, A., Amosse, Y., Soulevant, D., Senecat, P., Abart, J., and Paillart, P., "Generation of vertical gusts in a transonic wind tunnel," *Experiments in Fluids*, Vol. 56, No. 7, 2015, pp. 1–16. https://doi.org/10.1007/s00348-015-2016-5.

[25] Saddington, A., Finnis, M., and Knowles, K., "The characterisation of a gust generator for aerodynamic testing," *Proceedings of the Institution of Mechanical Engineers, Part G: Journal of Aerospace Engineering*, Vol. 229, No. 7, 2015, pp. 1214–1225. https://doi.org/10.1177/0954410014548237.

[26] Allen, N. J., and Quinn, M., "Development of a transonic gust rig for simulation of vertical gusts on half-models," *31st AIAA Aerodynamic Measurement Technology and Ground Testing Conference*, 2015. https://doi.org/10.2514/6.2015-2403.

[27] Fonte, F., Riccobene, L., Ricci, S., Adden, S., Martegani, M., et al., "Design, manufacturing and validation of a gust generator for wind tunnel test of a large scale aeroelastic model," *30th Congress of the International Council of the Aeronautical Science, Daejeon*, 2016, pp. 25–30.

[28] Poudel, N., Yu, M., Smith, Z. F., and Hrynuk, J. T., "A combined experimental and computational study of a vertical gust generator in a wind tunnel," *AIAA Scitech 2019 Forum*, 2019, p. 2166. https://doi.org/10.2514/6.2019-2166.

[29] Olson, D. A., Naguib, A. M., and Koochesfahani, M. M., "Development of a Low-Turbulence Transverse-Gust Generator in a Wind Tunnel," *AIAA Journal*, Vol. 59, No. 5, 2021, pp. 1575–1584. https://doi.org/10.2514/1.J059962.

[30] Reed III, W. H., *Aeroelasticity matters: Some reflections on two decades of testing in the NASA Langley transonic dynamics tunnel*, NASA TM-83210, 1981.

[31] Tang, D., Cizmas, P. G., and Dowell, E., "Experiments and analysis for a gust generator in a wind tunnel," *Journal of Aircraft*, Vol. 33, No. 1, 1996, pp. 139–148. https://doi.org/10.2514/3.46914.

[32] Roadman, J., and Mohseni, K., "Gust characterization and generation for wind tunnel testing of micro aerial vehicles," *47th AIAA Aerospace Sciences Meeting*, 2009. https://doi.org/10.2514/6.2009-1290.

[33] Makita, H., and Sassa, K., "Active turbulence generation in a laboratory wind tunnel," *Advances in turbulence 3*, Springer, 1991, pp. 497–505. https://doi.org/10.1007/978-3-642-84399-0_54.

[34] European Aviation Safety Agency, "Certification Specifications and Acceptable Means of Compliance for Large Aeroplanes CS25," , 2020. https://www.easa.europa.eu/sites/default/files/dfu/CS-25%20Amendment%2024.pdf, Last accessed on 18-03-2022.

[35] Akbari, M., and Price, S., "Simulation of dynamic stall for a NACA 0012 airfoil using a vortex method," *Journal of fluids and structures*, Vol. 17, No. 6, 2003, pp. 855–874. https://doi.org/10.1016/S0889-9746(03)00018-5.

[36] McCroskey, W., Carr, L., and McAlister, K., "Dynamic Stall Experiments on Oscillating Airfoils," *AIAA Journal*, Vol. 14, No. 1, 1976, pp. 57–63. https://doi.org/10.2514/3.61332.

[37] Choudhry, A., Leknys, R., Arjomandi, M., and Kelso, R., "An insight into the dynamic stall lift characteristics," *Experimental Thermal and Fluid Science*, Vol. 58, 2014, pp. 188–208. https://doi.org/10.1016/j.expthermflusci.2014.07.006.

[38] Leishman, G. J., *Principles of helicopter aerodynamics with CD extra*, Cambridge university press, 2006.

[39] Sheldahl, R. E., and Klimas, P. C., "Aerodynamic characteristics of seven symmetrical airfoil sections through 180-degree angle of attack for use in aerodynamic analysis of vertical axis wind turbines," Tech. rep., SAND 80–2114, Unlimited Release, UC-60, 1981.

[40] Manolesos, M., Papadakis, G., and Voutsinas, S., "An experimental and numerical investigation on the formation of stall-cells on airfoils," *Journal of Physics: Conference Series*, Vol. 555, IOP Publishing, 2014, p. 012068. https://doi.org/10.1088/1742-6596/555/1/012068.

[41] McAlister, K. W., Carr, L. W., and McCroskey, W. J., *Dynamic stall experiments on the NACA 0012 airfoil*, NASA TP 1100, 1978.

[42] Pullin, D., and Perry, A., "Some flow visualization experiments on the starting vortex," *Journal of Fluid Mechanics*, Vol. 97, No. 2, 1980, pp. 239–255. https://doi.org/10.1017/S0022112080002546.

[43] Das, D., Bansal, M., and Manghnani, A., "Generation and characteristics of vortex rings free of piston vortex and stopping vortex effects," *Journal of Fluid Mechanics*, Vol. 811, 2017, pp. 138–167. https://doi.org/10.1017/jfm.2016.733.

[44] Jaffe, A. M., "The millennium grand challenge in mathematics," *Notices of the AMS*, Vol. 53, No. 6, 2006, pp. 652–660.

[45] Wright, J. R., and Cooper, J. E., *Introduction to aircraft aeroelasticity and loads*, Vol. 20, John Wiley & Sons, 2008.